

# Modelling the functional dependency between root and shoot compartments to predict the impact of the environment on the architecture of the whole plant: methodology for model fitting on simulated data using Deep Learning techniques

Abel Louis Masson<sup>1</sup>, Yves Caraglio<sup>2,3</sup>, Eric Nicolini<sup>2,3</sup>, Philippe Borianne<sup>2,3</sup> and Jean-Francois Barczi<sup>2,3,\*</sup>

<sup>1</sup>AgroParisTech, F-78850, Thiverval-Grignon, France

<sup>2</sup>CIRAD, UMR AMAP, F-34398 Montpellier, France

<sup>3</sup>AMAP, Univ Montpellier, CIRAD, CNRS, INRAE, IRD, Montpellier, France

\*Corresponding author's e-mail address: [barczi@cirad.fr](mailto:barczi@cirad.fr)

Guest Editor: Andrea Schnepf

Editor-in-Chief: Stephen P. Long

Handling Editor: Andrea Schnepf

**Citation:** Masson AL, Caraglio Y, Nicolini E, Borianne P, Barczi J-F. 2021. Modelling the functional dependency between root and shoot compartments to predict the impact of the environment on the architecture of the whole plant: methodology for model fitting on simulated data using Deep Learning techniques.

*In Silico Plants* 2021: diab036; doi: 10.1093/insilicoplants/diab036

## ABSTRACT

Tree structural and biomass growth studies mainly focus on the shoot compartment. Tree roots usually have to be taken apart due to the difficulties involved in measuring and observing this compartment, particularly root growth. In the context of climate change, the study of tree structural plasticity has become crucial and both shoot and root systems need to be considered simultaneously as they play a joint role in adapting traits to climate change (water availability for roots and light or carbon availability for shoots). We developed a botanically accurate whole-plant model and its simulator (RoCoCau) with a linkable external module (TOY) to represent shoot and root compartment dependencies and hence tree structural plasticity in different air and soil environments. This paper describes a new deep neural network calibration trained on simulated data sets computed from a set of more than 360 000 random TOY parameter values and random climate values. These data sets were used for training and for validation. For this purpose, we chose VoxNet, a convolutional neural network designed to classify 3D objects represented as a voxelized scene. We recommend further improvements for VoxNet inputs, outputs and training. We were able to teach the network to predict the value of environment data well (mean error < 2 %), and to predict the value of TOY parameters for plants under water stress conditions (mean error < 5 % for all parameters), and for any environmental growing conditions (mean error < 20 %).

**KEYWORDS:** Calibration; Deep Learning; FSPM; root/shoot; whole plant.

## 1. INTRODUCTION

Plant growth modelling can be useful to predict plant biomass production and to study biological processes that take place throughout the lifetime of the plant. When studying plant biomass, it is important not

to forget the hidden part, the root system, which is required not only as a resource provider for plant survival but also stores a non-negligible proportion of plant biomass. In this study, we focus on process-based plant growth modelling applied to the whole plant, i.e. roots and shoots,

as opposed to statistical-based or allometric-based modelling. This kind of modelling describes the processes that explain plant behaviour. It was first applied to cultivated agronomic and forest species and mostly focussed on biomass production. These studies included a very rough description of the structure (King 1991; Friend 2001; Buck-Sorlin 2013). On the other hand, many models represent plant structure. Concerning the aerial parts, de Reffye *et al.* (1988), Kurth (1994) and Smith *et al.* (2014) show the 3D shape of trees with varying degrees of botanical accuracy. Concerning roots, Pages (1999), Leitner *et al.* (2010) and Postma *et al.* (2017) provide models but these are mostly dedicated to monocotyledons. All these models make it possible to study interactions between one compartment and its environment (for instance, shoot vs. light or roots vs. soil). Studies on tree growth including both structure and biomass (functional–structural plant models, FSPMs) have mainly been carried out on shoot systems in agronomic and forest species (Vos *et al.* 2007, 2010; Sievanen *et al.* 2009; Reyes 2020; de Reffye *et al.* 2021). Particular attention has been paid to the influence of light in Buck-Sorlin *et al.* (2011) and hydraulics properties in Braghieri *et al.* (2020). The root system is usually taken apart due to the difficulties involved in observing and measuring it, especially root growth. However, climate change has made it crucial to study the structural plasticity of trees including root/shoot interactions. For this purpose, both shoot and root compartments must be considered simultaneously as they play collaborative roles with respect to climate traits (water availability for roots and light or carbon availability for shoots). Bornhofen and Lattaud (2007) proposed a theoretical model of whole trees to explain species evolution; however, it was only sketchy, far from the real plant architecture. Lachenbruch and McCulloch (2014) and Ledo *et al.* (2018) also published whole tree studies but these contained simplified description of tree structure.

The question we aimed to answer with the present study is: what is plant plasticity with respect to biomass production and partitioning considering both shoot and root systems?

The production of biomass is the basis for the growth of both above- and below-ground tree axes. However, trees have the capacity to favour the growth of certain axes at the expense of others (e.g. trunk, stump), by partitioning biomass between the root and shoot compartments. Moreover, biomass partitioning has been shown to be driven by the resource that limits biomass production (Liu *et al.* 2012; Hertel *et al.* 2013). For example, under water stress, the tree allocates a larger share of the biomass produced to the root system, thus allowing more absorption of water. On the other hand, under light stress, the tree allocates a larger share of the biomass to the shoot system, thus allowing better absorption of light. The effects of drought are widely documented in the literature (Hommel *et al.* 2016; Ledo *et al.* 2018), light (Ballare and Pierik 2017) as are the effects of nutrient availability (Reynolds and D'Antonio 1996; Poorter *et al.* 2012) on biomass partitioning between root and shoot systems. For a review, see Poorter *et al.* (2012). More generally, here we consider the ability of the tree to adapt to resource availability by modulating biomass partitioning as defined in optimal partitioning theory (Niklas and Enquist 2002; Reich 2002; Colter Burkes *et al.* 2003): resources are allocated to both compartments in order to balance their contribution capabilities.

First we present a model and its simulator which merges the DigR root model (Barczi *et al.* 2018) and AmapSim Caulinar model (Barczi

*et al.* 2008) to produce a whole-plant structural model we named RoCoCau (for Root, Collar, Caulinar). Since the architecture of both systems and the visible traits that express this partitioning are indispensable, RoCoCau was designed to mimic whole-plant growth with very good botanical accuracy.

Second, we present TOY, an external model and its simulator that is linked to RoCoCau. TOY represents shoot and root compartment dependencies and hence tree structural plasticity in different air and soil environments. The TOY model aims to describe links between the root and shoot systems for both the production and sharing of biomass when the plant is faced with a variable environment while simultaneously describing both compartments during growth with good botanical accuracy.

Before model validation, a recurrent question for any model is fitting. RoCoCau parameters are calibrated using traits directly measured in the field. The problem of model fitting was solved in previous studies (Barczi *et al.* 2008, 2018). On the other hand, most of the TOY model parameters are hidden, meaning they cannot be measured directly. In this paper, we calibrate 25 numerical values for the TOY model, which is a huge number for common fitting methods (least square, simulated annealing, genetic algorithm, etc.). The solution space is very wide and standard methods may be captured in local minima. Some model inversions have already been tried (Matsunaga *et al.* 2001; Higgins *et al.* 2010; de Reffye *et al.* 2016), but they targeted a small number of hidden parameters that cannot be directly measured on the plant. In this paper, we describe our experimental calibration using a convolutional neural network. This technique is mainly used for object detection or classification from numerical images, but is sometimes used in a generative way to predict parameter values for model calibration (Danson *et al.* 2003; Bacour *et al.* 2006; Su *et al.* 2015; Song and Xia 2016; Qi *et al.* 2016).

Another difficulty when fitting the TOY model is the lack of experimental data, especially on root system architecture. The architectural traits of a root system can only be measured through destructive methods involving the uprooting of the tree, which for logistic reasons, hinders the creation of data sets that are large enough to allow the training of a neural network using real data. To validate our claim that RoCoCau can produce simulated trees that are close to reality, we use standard traits (shoot length/root growth speed, branching density, geometry, etc.) to calibrate RoCoCau on particular species and we then calibrate the TOY model using simulated data sets to train a neural network.

## 2. MATERIALS AND METHODS

### 2.1 Model

The aim of RoCoCau+TOY FSPM is to predict and simulate the impact of the environment, particularly resource availability, on whole-plant architectural development. The RoCoCau structural model enables accurate simulation of whole-plant architectural development, based on a few architectural measurements. However, RoCoCau does not explicitly model the functional processes that drive architecture development. These include both endogenous (genetic) and exogenous (environment) functional processes and prevent RoCoCau from simulating the impact of the environment on whole-plant architectural development. We designed the TOY model to (i) disentangle the effects of genotype and environment on whole-plant architectural

development, (ii) predict the impact of environmental constraints, especially water and light availability, on biomass partitioning between the root and shoot compartments, (iii) plug in to RoCoCau, allowing RoCoCau+TOY FSPM to simulate the development of whole-plant architecture with respect to these functional constraints.

### **2.1.1 RoCoCau—a structural model to simulate whole-plant growth.**

Field experiments and observations led us to develop a whole-plant model and its simulator named RoCoCau. This pure structural model is the result of merging two existing structural models; a model for the shoot system, AmapSim (Barczi *et al.* 2008) and a model for the root system, DigR (Barczi *et al.* 2018). Whole-plant architecture development is modelled as a set of virtual shoot and root meristems, whose development is driven by stochastic processes that represent apical growth (axis elongation), lateral growth (branching) and death. For the shoot system, the value of the parameters of these processes varies with the physiological age (partially expressed by the term ‘vigour’) of each virtual shoot apical or lateral meristem. The shoot system is described as a topology of shoots belonging to different categories. The physiological age of each shoot meristem evolves along a reference axis defining the different possible values of physiological age according to an oriented finite automaton whose law of occupation and transition follows a semi-Markovian function (Barczi *et al.* 2008; de Reffye *et al.* 2021). The root system is described as a topology of roots belonging to different categories in the same way as the shoot. The vigour of a root meristem depends on the type of root and on the current length of the root (Barczi *et al.* 2018). The geometry of the resulting axes is then modelled using simple descriptive functions. The stochasticity of the processes modelling the development and the differentiation of each axis implies the uniqueness of each simulated axis. Nevertheless, it is possible to classify axes in distinct structural categories according to their morphological specificity and to define the way these structural categories are combined into shoot and root branching systems (i.e. architectural units; Barthélémy and Caraglio 2007). Both models produce botanically accurate shapes obtained by calibrating their parameters using measurements taken on real plants. The models were tested and validated on many plant species (Barczi *et al.* 2008, 2018). The simulator of RoCoCau combines the AmapSim and DigR simulators in a single program in which all shoot and root meristems are synchronously simulated with a software architecture that allows external models that can interact with the default simulation kernel to be plugged in (Barczi *et al.* 2008).

### **2.1.2 RoCoCau+TOY, an FSPM to simulate the impact of environmental constraints on the development of whole-plant architecture.**

RoCoCau is a purely structural model which incorporates both endogenous (i.e. growth and branching patterns according to structural categories of axes) and exogenous effects on the growth of the whole plant. To disentangle the two effects, we developed TOY, an extra model that represents (i) biomass production according to current plant structure and environmental constraints, (ii) biomass partitioning and its influence on plant growth and architectural development. Within TOY, functional dependency is modelled only at the compartment level, i.e. between the root and shoot compartments. Within each compartment, the role of the axes can be associated with three main functions: structuring, exploration and exploitation. This is the

reason why, in TOY, we arbitrarily created six independent functional categories for the axis (three for the shoot compartment and three for the root compartment) according to the function to which they contribute the most. For instance, for the shoot system, the first functional category, grouping the axes that mostly contribute to the structuring function includes the trunk and main forking branches; the second functional category, grouping the axes that mostly contribute to exploration includes the other branches; the third functional category, grouping the axes that mostly contribute to exploitation includes the short shoots. It is important to note that the functional categories can include several structural categories. It is up to the modeller to define the architectural units of the shoot and root systems (i.e. structural categories and their relative organization). For RoCoCau settings and for TOY settings, it is also up to the modeller to define the content of each of the six functional categories in terms of structure. The flexibility of this approach makes it possible simulate a wide range of architectures considering both structure and function. Figure 1 shows a simple example of a shoot/root architectural unit and a shoot growth loop. In the rest of this paper, it is important to clearly distinguish between the structural axis categories (a classification defined in RoCoCau) and the functional axis categories (a classification defined in TOY).

The software implementation of RoCoCau enables dynamic linking of plug-ins that contain additional knowledge that will interact with the default RoCoCau algorithm. TOY plug-in processes take place in two different modes (Fig. 2). (i) At the end of each simulation time step, RoCoCau stops simulating growth and the TOY plug-in takes over. Knowing the actual shape of the tree and the quality of the environment (water and light), TOY computes biomass production, partitioning and the resulting growth attenuation factors. It then hands back to RoCoCau. (ii) In the following time step, RoCoCau uses the TOY actual attenuation factors to moderate apical growth, branching and death of meristems depending on which compartment and which functional category they belong to.

### **2.1.3 Description of the TOY model.**

The growth of the whole plant is the result of endogenous processes, driven by the expression of the plant’s genotype, and of exogenous processes, driven by the interaction between the plant and its environment. In simulations, each time step usually represents a year of growth. Exogenous processes are updated at the beginning of each time step, and endogenous processes are called on throughout the duration of the time step for the simulation of the growth of each axis. In the TOY model, the environment is defined as a set of three parameters, representing light (useable light energy,  $Light\text{ (w}\cdot\text{m}^{-2}\text{)}$ ), inorganic carbon (concentration of atmospheric carbon,  $C_{air}$ ) and water (soil relative humidity by volume,  $Hv_{soil}$ ) resources.

Exogenous growth processes, namely absorption of resources, sugar production and partitioning between the root and shoot compartments, are modelled by a set of equations using four parameters:  $k$ ,  $Light_{max}$ ,  $R_{||}$  and  $RAL$ . The light extinction coefficient  $k$ , and the maximum useable light energy  $Light_{max}$  ( $\text{w}\cdot\text{m}^{-2}$ ) are parameters of the light absorption equation. As inspired by Nye (1973) and Jungk (2001), the root absorbing length ( $RAL$ ) represents the length of the apical absorbing part of the roots and the  $R_{abs}$  radius of the volume of soil investigated. We are aware that our representation of the soil

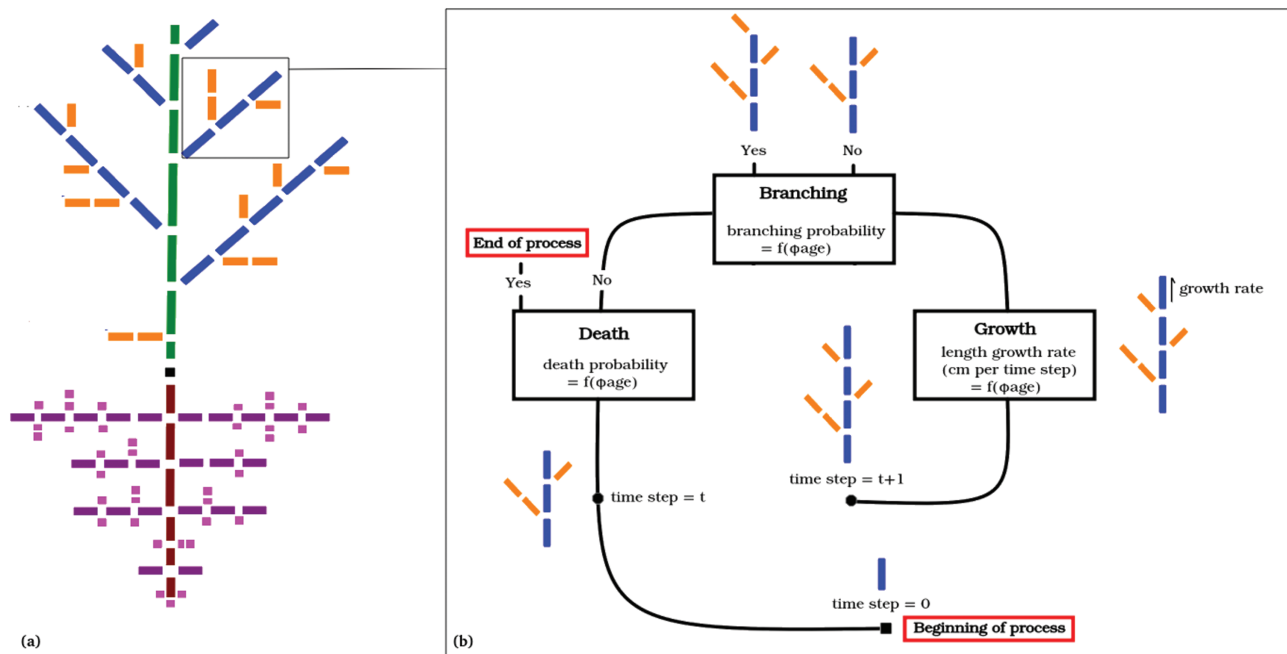


**Figure 1. Plant structure and growth algorithm.** (A) The plant as a branched system of axes belonging to different structural categories (e.g. trunk, branches and short axes; taproot, lateral roots and fine roots), that can be grouped in six functional categories, three for each compartment, e.g. structuring category (green: shoot system, dark red: root system); blue, purple: exploration category; orange, pink: exploitation category. (B) Shoot axis development process implemented by RoCoCau (simplified). Φage stands for the physiological age of the virtual meristem.

and of water transfer are very rough compared to those of [Doussan et al. \(2006\)](#) and [Garrigues et al. \(2006\)](#), but our aim is to describe the different processes that occur in the plant at the same level of detail. Modelling exogenous processes also requires whole-plant variables that are provided by RoCoCau: leaf surface area ( $S_{leaves}$ ), which represents the sum of the surface area of all leaves, leaf area index  $LAI$ , the radius of the root absorbing soil  $R_{abs}$  and  $RAL$ .

Endogenous processes regulate the growth, branching and death of the axes. The processes are specific to each axis functional category and are modelled by a threshold function with three parameters:  $S_m$  the mortality threshold,  $S_r$  the branching threshold and  $A_l$  the apical growth factor. Since the TOY model distinguishes six-axis functional categories, the total number of parameters used by the TOY model is 25 ( $7 + 6 * 3$ ).

The TOY model functions in four successive stages: (i) estimating sugar production according to light, carbon and water resources, under actual and optimal environmental conditions, (ii) estimating actual and optimal sugar partitioning, i.e. estimating the quantity of sugar allocated to the root and shoot compartments, under actual and optimal environmental conditions, (iii) comparing the actual and optimal sugar partitioning in each compartment to estimate the distance between actual and optimal growth conditions (growth factor), (iv) for each axis, the functional category within each compartment, determining the response of the axes to the distance between actual and optimal growth conditions (growth factor), i.e. determining the impacts of a reduction in the quantity of sugar allocated, under actual

growth conditions, on the death, branching and growth processes of the axis. We now detail each of the four steps.

(i) The production of sugar by photosynthesis is calculated as a function of the quantities of water, carbon and light absorbed. Carbon absorption is modelled as the product of leaf surface and the concentration of carbon in the air  $Carbon(t) = S_{leaves}(t) \times C_{air}$ ; water absorption is modelled as the product of the volume of the absorbing parts of the roots and soil relative humidity  $Water(t) = V(t) \times H_{soil}$ , with  $V(t) = \pi \times R_{abs}^2 \times \sum_{allroots} min(Rootlength(t), RAL)$ ; light absorption is modelled as the product of available light energy  $Light(t)$  ( $w \cdot m^{-2}$ ) and photosynthetic efficiency, which can be represented by a decreasing exponential as a function of the leaf area index  $LAI(t)$  and the light extinction coefficient  $k$ . Sugar production is assumed to be controlled by the limiting resource (the minimum between absorbed water and carbon quantities).

$$Sugar(t) = min(Water(t), Carbon(t)) \times Light(t) \times exp^{-k \times LAI(t)} \quad (1)$$

Optimal environmental conditions are defined as soil relative humidity equal to 1, i.e.  $Water_{max}(t) = 1$ , and light absorption equal to maximum useable light energy  $Light_{max}$  ( $w \cdot m^{-2}$ ). According to [equation \(1\)](#), optimal sugar production  $Sugar_{max}(t)$  is then:

$$Sugar_{max}(t) = min(V(t), Carbon(t)) \times Light_{max} \times exp^{-k \times LAI(t)} \quad (2)$$

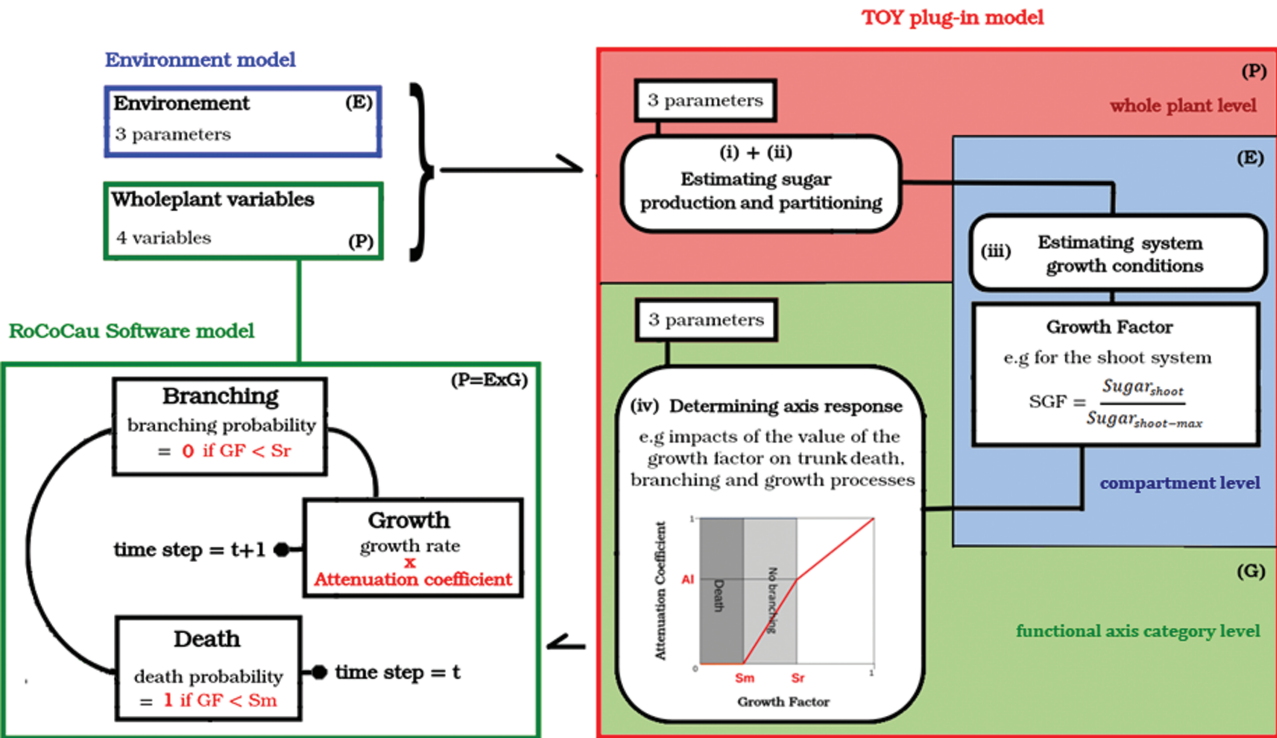


Figure 2. Schematic representation of the functioning of RoCoCau+TOY FSPM: the colours refer to the specificity of the modelling process; red for processes that occur at whole-plant level, blue for processes specific to each compartment (root and shoot) and green for processes specific to each development based on the filling of the zones of a segmented 3D image with the voxelized density maps of each successive plant structure.

(ii) According to the optimal partitioning theory, the partitioning of sugar production between the root and shoot compartments is assumed to be inverse to the contribution to production. Sugar partitioning between root and shoot is then calculated as follows:

$$\begin{cases} Sugar_{shoot}(t) = Sugar(t) \times \frac{Water(t)}{Carbon(t)+Water(t)} \\ Sugar_{root}(t) = Sugar(t) \times \frac{Carbon(t)}{Carbon(t)+Water(t)} \end{cases} \quad (3)$$

According to equation (2) optimal partitioning of sugar production is:

$$\begin{cases} Sugar_{shootmax}(t) = Sugar_{max}(t) \times \frac{Water_{max}(t)}{Carbon(t)+Water_{max}(t)} \\ Sugar_{rootmax}(t) = Sugar_{max}(t) \times \frac{Carbon(t)}{Carbon(t)+Water_{max}(t)} \end{cases} \quad (4)$$

(iii) For each compartment, the distance between actual and optimal growth conditions is estimated by calculating its growth factor; i.e. the ratio of the quantity of sugar allocated under actual growth conditions to the quantity of sugar allocated under optimal growth conditions.

$$GrowthFactor_{compartment}(t) = \frac{Sugar_{compartment}(t)}{Sugar_{compartmentmax}(t)} \quad (5)$$

(iv) For each axis functional category in each compartment, the response of an axis to the distance between actual and optimal growth conditions, i.e. the impacts of the value of the growth factor

on axis death, branching and growth processes, are modelled by a threshold and attenuation function (TAF; Fig. 3). When the value of the growth factor is equal to 1, the growth of the axis is not attenuated. When the value of the growth factor is less than 1 and more than the branching threshold  $S_r$ , the growth rate of the axis is attenuated by a coefficient that decreases linearly with the value of the growth factor, according to the values of  $S_r$  and the apical growth factor  $A_l$ . Then, when the value of the growth factor falls below the branching threshold  $S_r$ , the axis stops branching, and the attenuation coefficient decreases linearly with the value of the growth factor, according to the values of  $S_r$ ,  $A_l$  and the mortality threshold  $S_m$ . Finally, when the value of the growth factor falls below the value of the mortality threshold  $S_m$ , the axis dies.

## 2.2 Model calibration

The main difficulty in disentangling exogenous and endogenous growth processes is providing an adequate description of endogenous growth processes, and more specifically in estimating parameter values for endogenous growth equations. Indeed, endogenous effects on plant architecture are (i) inherently more difficult to observe and measure and (ii) perceivable only by monitoring the whole plant's architectural development over time. Standard calibration of the 18 TOY hidden parameter values for endogenous growth (Table 1), relying on simple relationships between parameter values and measurement of specific architectural traits is therefore impossible. In this section we present

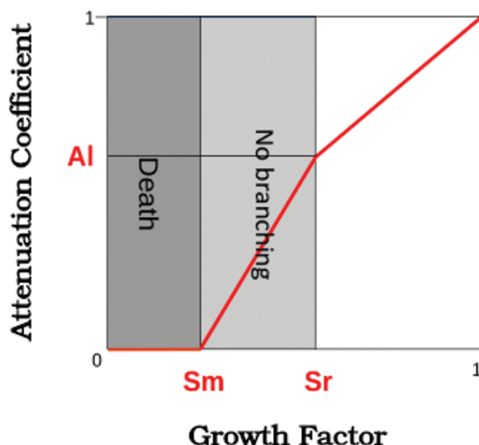


Figure 3. Threshold and attenuation function (TAF).

a method for the calibration of the 18 TOY hidden parameters for endogenous growth.

Since the model is still in the early stages of development, the aim of this section is rather to address the main difficulties encountered in calibration than to provide complete calibration of the model. As the parameters for exogenous growth can be calibrated using standard calibration techniques, we do not carry out this task here, but this issue is addressed in the discussion section.

**2.2.1 Model calibration on simulated data using Deep Learning techniques.** The most efficient way to calibrate TOY hidden parameters, as performed in Cournede *et al.* (2011) and de Reffye *et al.* (2018), is model inversion, so as to define a method enabling assessment of the input parameter values from the simulated plant architectural development. Generative deep neural networks can learn the intricate relationship between each parameter value and plant architecture development over time. Provided with an input consisting of a representation of plant architecture development over time, they can assess TOY model parameter values.

Generative deep neural networks can be trained on a simulated training data set, with each example of the training data set consisting of a simulation of the plant's architectural development by the RoCoCau+TOY FSPM, labelled with the values of TOY model parameters.

The two main choices to be made for this method of calibration are the choice of a suitable representation for the simulations of the plant's architectural development, and the choice of a suitable architecture for the deep generative neural network. Indeed, the simulations of a plant's architectural development must be in a format that can be processed by a deep neural network. The chosen representation must introduce as little bias as possible and must be obtained from a simulation as fast and easily as possible to be able to build a large training data set. The chosen network architecture must be able to learn the link between the representation of plant architectural development and TOY parameter values rapidly and with the best possible accuracy.

Table 1. TOY model parameters used to model environment, exogenous and endogenous growth. Environment parameters are averages over one time step. They can either be constant throughout the simulation, i.e. no variability, or vary according to the time step of the simulation.

	Symbol	Name		Unit	Estimation
Environment	$C_{air}$	Concentration of inorganic carbon in the air		ppm	Measured or fixed by the modeller
	$Light$	Useable light energy		$w \cdot m^{-2}$	Measured or fixed by the modeller
	$Hv_{soil}$	Relative soil humidity as a function of volume		dimensionless 0 to 1	Measured or fixed by the modeller
Exogenous growth	$k$	Light extinction coefficient		dimensionless	Estimated from measurements or given in the literature
	$Light_{max}$	Theoretical maximum useable light energy		$w \cdot m^{-2}$	Measured or fixed by the modeller
	$R_{abs}$	Radius of the volume of absorbing soil		cm	Measured or fixed by the modeller
	$RAL$	Length of the apical absorbing part of the root		cm	Measured or given in the literature
Endogenous growth	Functional categories	$S_m$	Mortality threshold	dimensionless 0 to 1	Hidden parameter
		$S_r$	Branching threshold	dimensionless $S_m$ to 1	Hidden parameter
		$A_l$	Apical growth factor	dimensionless 0 to 1	Hidden parameter

**2.2.2 Choosing to represent plant architecture development over time as a voxelized density map that can be processed by the 3D deep convolutional neural network VoxNet.** One of the outputs of a plant's architectural development as simulated by the RoCoCau software is a time series of three-dimensional mock-ups. However, it is possible to get rid of the time dimension entirely by representing plant architecture development as a scene, by including the successive structures of the plant in the same 3D image.

Point or voxel clouds are already used in LiDAR data processing (Wandinger 2005; Côté *et al.* 2009; Mak and Hu 2015; Ferrara *et al.* 2018; Fan *et al.* 2020; Estornell *et al.* 2021; Mayra *et al.* 2021), and are a well-documented and efficient way to represent a three-dimensional plant structure. Voxel clouds are equivalent to point clouds, except that the point coordinates are fixed and equidistant from one another, thus avoiding potential bias and making it possible to define the necessary neighbourhoods to process convolution in neural networks. Moreover, non-binary voxels can have a value. This value can be used to describe the amount of plant biomass in the voxel's volume. This makes it possible to represent plant structure as a distribution of biomass in a 3D space, i.e. as a voxelized biomass density map.

Since it is relatively easy and quick to transform RoCoCau simulations into voxelized density maps, this representation can create a 360 000 simulation training data set in less than 2 days using a standard PC. Moreover, even if the voxels are large, the information in each voxel concerning the amount of biomass it contains makes it possible to obtain a relatively accurate representation of plant structure.

The VoxNet network presented in Maturana and Scherer (2015) is a deep 3D convolutional neural network, and is promising for 3D object recognition tasks (Maturana and Scherer 2015; Liu *et al.* 2021). The use of convolution by VoxNet makes it possible to rapidly process 3D images such as voxelized density maps, which could be too big for non-convolutional networks. VoxNet was originally developed to predict the class label of a 3D object from its occupancy grid, but it can be adapted to generate parameter values from a voxelized density map representing plant architectural development.

The VoxNet network is also particularly well suited for processing point cloud (for instance, LiDAR) data (Maturana and Scherer 2015) after conversion to voxel data. This makes it possible to use it not only for calibration on simulated data, but also for calibration on real data acquired with LiDAR.

**2.2.3 Pre-processing the simulation of architecture development by RoCoCau, to be used as inputs for VoxNet** Representing plant architectural development as a voxelized density map requires the definition of a unique pre-processing procedure that can transform a simulation by the RoCoCau software into a voxelized density map (Fig. 4). In this study, the simulations provided by the RoCoCau software are performed in 10 time steps, representing 10 successive plant structures. To be compatible with the VoxNet network input format, the size of the 3D image containing the voxelized density map is fixed at 30 × 30 × 30 voxels. For each simulation, the pre-processing procedure relies on (i) the voxelization of the 10 successive structures of the RoCoCau simulation, and (ii) the segmentation of the 3D image into 10 time-specific zones to host these structures at 10 successive ages.

Since the TOY model relies on absorbing zones (leaves and absorbing roots) for biomass production and on woody parts for growth control, TOY calibration takes advantage of separating these two traits to make calibration more efficient.

(i) Each successive structure of the plant is separated into two, providing two substructures for the absorbing parts (leaves and absorbing roots) and for the woody parts (branches and roots) of the plant. Each substructure is then placed in a 3D space made up of voxels of whose sides measure 20 cm. Each voxel is assigned a value according to the amount of plant biomass within its volume. Two voxels within the 3D space accommodating the woody substructure are attributed values representing water and light availability. This voxelization procedure makes it possible to obtain a voxelized density map of a single plant structure.

(ii) The 3D image is separated into two equal halves, on the left (resp. right) for the accommodation of absorbing (resp. woody) substructures. Each half is then divided into 10 time zones of appropriate size to accommodate each of the 20 voxelized substructures. Filling the time zones of this segmented image with the previously voxelized substructures, with respect to their chronological order, enables production of a voxelized density map of plant architectural development.

**2.2.4 Training VoxNet to predict TOY hidden parameter values** The calibration of the TOY model is not a classification problem (Fig. 5A). As it was originally developed to classify 3D objects, the architecture of VoxNet was adapted to predict TOY hidden parameter values. Adaptation concerned the fully connected layer and the loss function, which is set as the root mean square error (RMSE). To optimize speed and quality and thanks to the independence of the functional categories of the six axes defined in the TOY model, VoxNet was trained six times, each training run for one of the functional categories and aimed to predict their three parameter values. For this purpose, the size of the fully connected layer was reduced to three. The final result consists of six trained VoxNets, each having a set of weights computed to predict the three parameters of each of the functional categories.

According to the recommendation for the use of VoxNet (Maturana and Scherer 2015), the size of the training data set was set to 300 000 examples belonging to the same species which means that RoCoCau parameters were fixed to describe a particular species. The creation of the training data set followed a four-step procedure: (i) generating random values for TOY parameters; (ii) simulating plant architecture development over 10 time steps with RoCoCau+TOY FSPM using the TOY generated parameter values; (iii) pre-processing simulations of plant architectural development following the pre-processing procedure described above and labelling each voxelized density map with the three parameter values that VoxNet will have to predict; (iv) converting the resulting examples into a training-friendly format (.npy) (Maturana and Scherer 2015).

Since a single training run allows the prediction of three parameter values, the prediction of TOY 18 hidden parameter values requires six training runs. Beyond improving the quality and increasing the speed of each individual training run, this division also enables fine-tuning. Once a training has been performed, e.g. for the first shoot functional category, it is indeed possible to speed up the

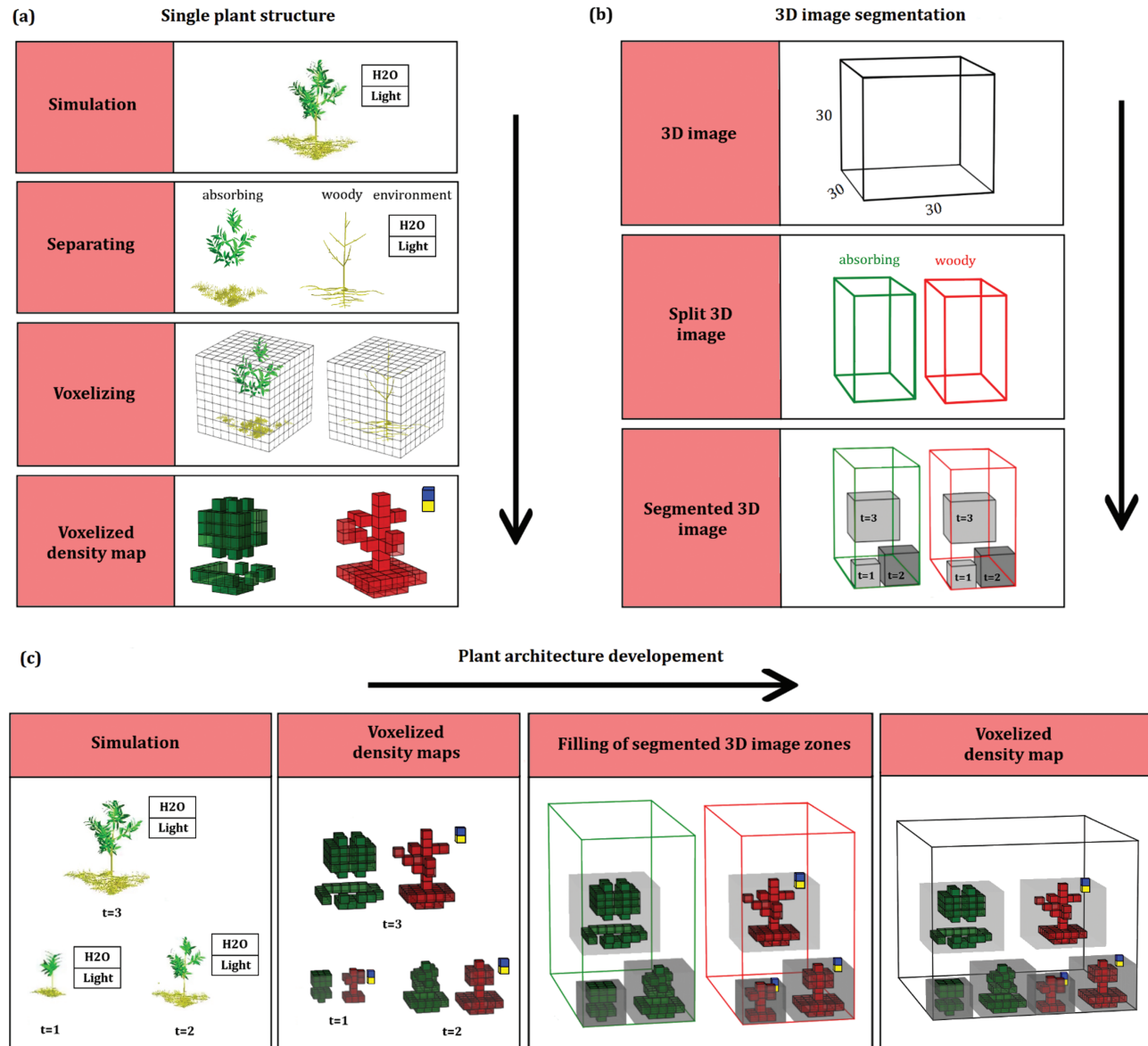


**Figure 4. Voxelization flowchart.** From of a simulation of plant architectural development to a voxelized density map that can be used as an input for the VoxNet neural network. In each image, the colours represent the nature of the information contained in the voxel: green for absorbing biomass, red for woody biomass, blue for water availability and yellow for light availability. The brightness of the green and red voxels is set to represent the value they contain: the greater the value, the brighter the voxel. For aesthetic reasons in this example, the number of time steps for the simulation of architecture development was fixed at three. (A) Voxelization of a single plant structure. (B) 3D image splitting and division into time-specific zones. (C) Voxelization of plant architectural development based on the filling of the zones of a segmented 3D image with the voxelized density maps of each successive plant structure.

remaining trainings, e.g. for the second and third shoot functional categories, by using the weights of the previously trained VoxNet as initial values.

*A priori*, since TOY parameters depict plant response to environmental stress, their values should be exceedingly difficult to predict from a representation of a plant architecture that has developed in a

stress-free environment. To avoid training failure, we isolated the sub-data set *SubDBStress* containing only examples in which the plant architecture developed under light and water stresses (reduction of at least 25 % in light availability and of at least 25 % in water availability compared to the optimum). Once a training run has been performed on *SubDBStress*, it is possible to avoid the failure of the training on

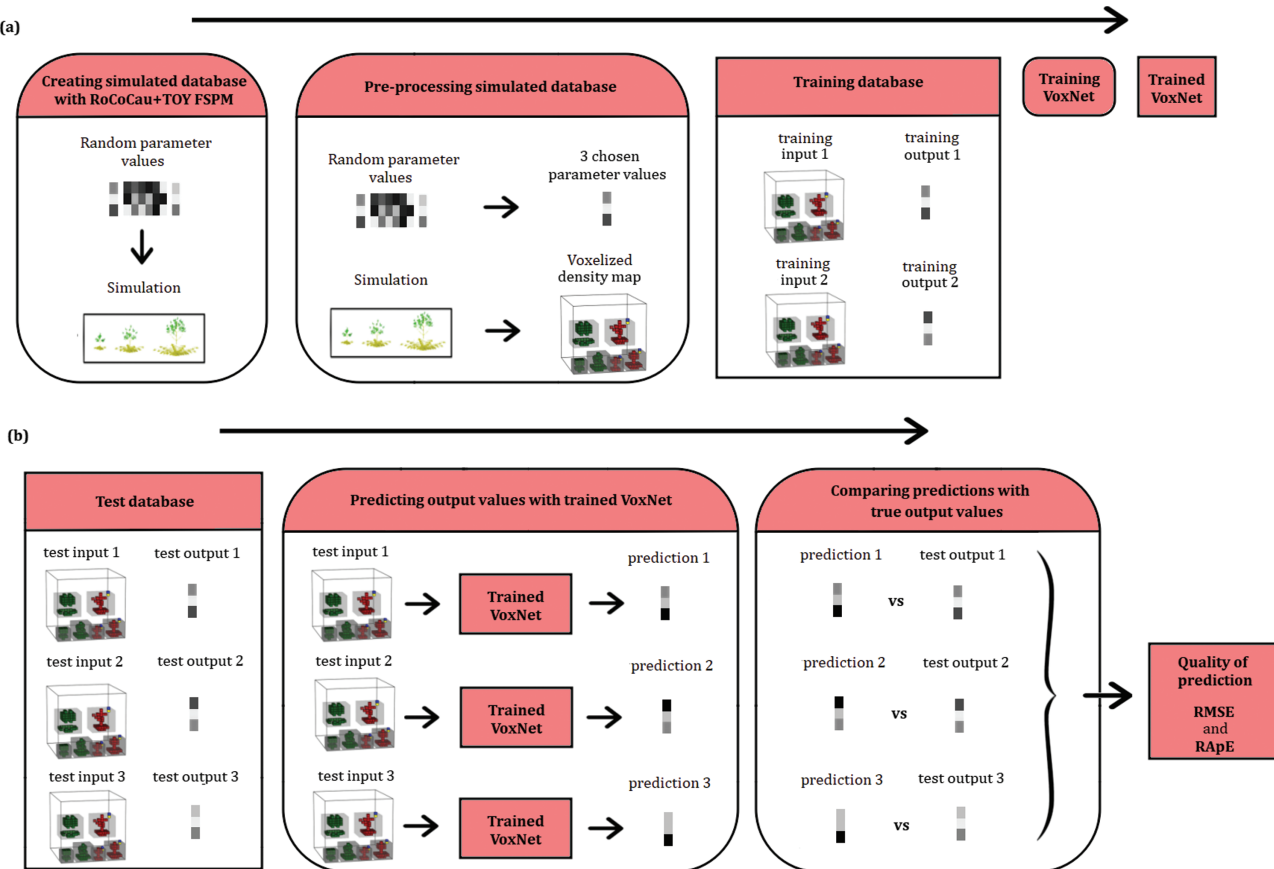


Figure 5. (A) Training VoxNet, from creating a training data set using RoCoCau+TOY to obtaining a trained VoxNet neural network. (B) Testing the quality of trained VoxNet predictions using a test data set.

the whole data set by using the weights of the VoxNet trained on *SubDBStress* for initialization.

Finally, the training procedure for the calibration of TOY 18 hidden parameters with fine-tuning followed three steps: (i) training two VoxNets to predict the three parameter values for the first shoot (resp. root) functional category on *SubDBStress*, (ii) training four VoxNets to predict the three parameter values of the second and third shoot (resp. root) functional categories on *SubDBStress* fine-tuned with the weights of the training on the first shoot (resp. root) functional category on *SubDBStress*, (iii) training six VoxNets to predict the three parameter values of each functional category on the whole data set, fine-tuned with the weights of the training on *SubDBStress*.

**2.2.5 Testing the quality of the prediction by trained VoxNet** In each training run, changes in the value of the training loss function (RMSE) were monitored to ensure the effective learning of VoxNet (Fig. 5B). Same monitoring was also carried out on the validation data set to avoid overfitting.

The quality of the training is tested on a test data set containing 400 test examples. For each example of the test data set, the input of the example, i.e. the voxelized density map is used as an input to the trained VoxNet. The trained VoxNet then delivers a prediction for

the values of the chosen set of three hidden parameters it has been trained to predict, e.g. the death threshold, the branching threshold and the apical growth factor (see Table 1). Its prediction is then compared with the output of the example, containing the true values of the three hidden parameters. The comparison is performed through an estimation of the RMSE, and the relative absolute percentage error (RApE) between each hidden parameter true and predicted values.

To test the quality of VoxNet predictions under contrasted environmental conditions, the test data set was divided into four sub-data sets, according to the severity of light and water stress under which the plant architecture of the example developed. Each training run was tested on the whole test data set as well as on each of the four test sub-data sets (see Results)

### 3. RESULTS

#### 3.1 RoCoCau+TOY FSPM use and analysis *in silico*

Depending on the modeller's knowledge of the tree species to be modelled, it is up to him/her to define the sensitivity of each of the six functional categories proposed by the TOY model. Combining the sensitivities of all six-axis functional categories defines the sensitivity of the whole plant. It will be recalled that we set the number of

functional categories based on the three main functional roles of the shoot or root axes, i.e. structuring, exploration and exploitation.

Once the RoCoCau model was set up to a particular species and the TOY model was set up and its simulator running, two kinds of tests were carried out to check its ability to mimic what is known about whole-plant functioning by: (i) testing the phenotypic plasticity of virtual plant species while varying the environment, (ii) testing the ability of the model to represent different plant strategies while varying the endogenous parameters of the six functional categories.

**3.1.1 Predicting phenotypic plasticity under varying environmental conditions** By varying the TOY parameter values, we tested the capacity of the TOY model to express plant plasticity in different environments. For instance, we programmed a plant with a second functional branch category (lateral in this case) with highly sensitive apical growth ( $A_l = 0$ ) while all the other shoot functional categories are less sensitive ( $A_l = 1$ ). This results in strong apical dominance under stress. In the below-ground compartment, the third root category (fine roots in this case) is set sensitive to death ( $S_m = 0.3$ ) while the other categories are not ( $S_m = 0.1$ ). The first functional root category (taproot in this case) has highly sensitive apical growth ( $A_l = 0$ ) while other functional root categories are less sensitive ( $A_l = 1$ ). This results in the plant being sensitive to drought. We simulated the growth of this theoretical plant using combinations of two light

conditions (maximum and half maximum) and two water conditions (maximum and half maximum). **Figure 6** shows the result of the four simulations. At first sight the differences between the shape of the same plant in different environments are clearly visible. Taking the plant with no stress as reference (lower right), we see that the plant facing light and water stress (upper left) is globally weaker and did not even branch in Years 8 and 9. Both root and shoot systems are small. We see that plants under light stress or water stress are smaller than the reference plant. We also see that the root/shoot ratio of plants under water stress is opposite to the ratio of the plant facing light stress. If we look at the numbers, the impression we got at first sight is confirmed. Plant under both stresses have fewer and shorter axes than the plant in optimal environment. The three other plants have the same number of branches but the plant under water stress has twice as many fine roots as the plant under light stress, which has shorter side branches.

**3.1.2 Generic modelling of genotype, defining plant sensitivity to environmental constraints** Three parameters of each of the six functional axis categories control its death ( $S_m$ ), branching ( $S_r$ ) and apical growth ( $A_l$ ) depending on the current value of the growth factor of the corresponding compartment. **Figure 7** shows four examples of the possible use of these three parameter values in the second category of branches (lateral branches). Parameter  $A_l$  controls apical growth

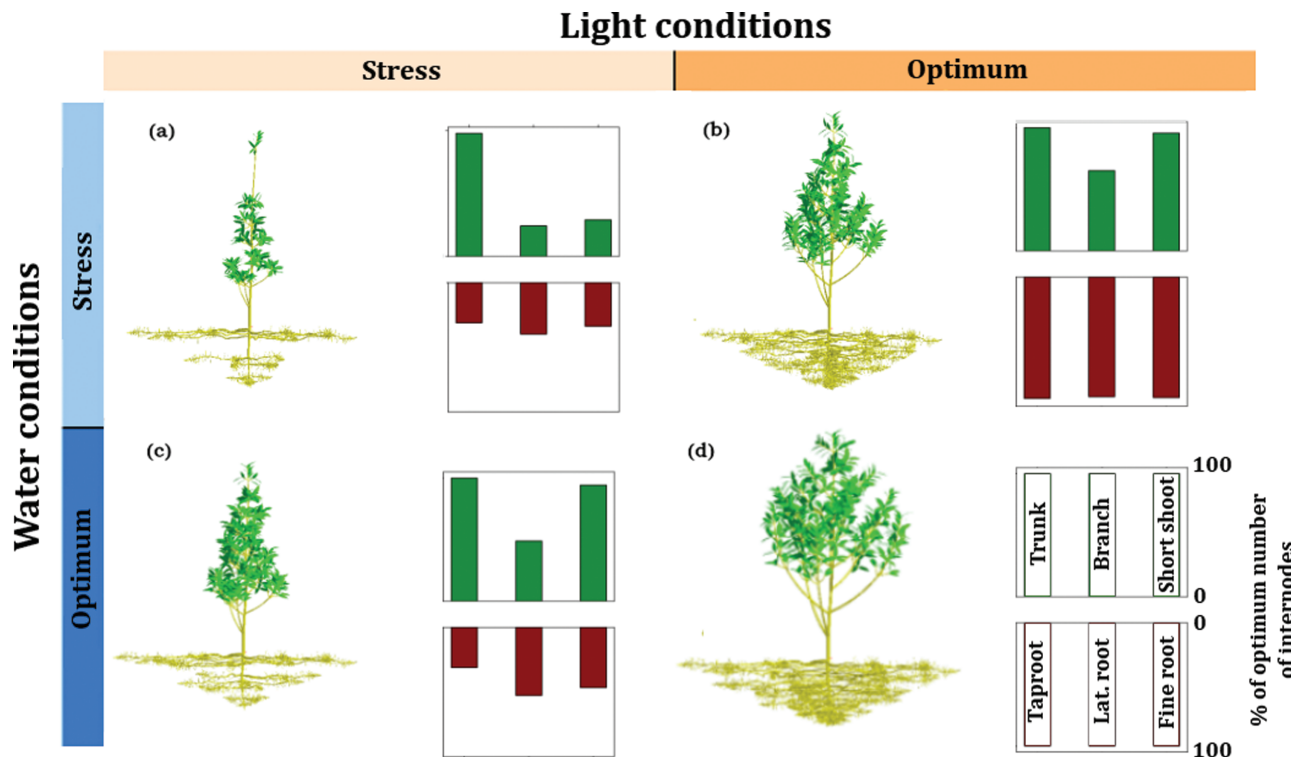


**Figure 6.** Results of four simulations of random plant architectural development with RoCoCau+TOY FSPM under different environmental water and light conditions. The number of internodes of the functional category of each axis were counted using Xplo Software. For each simulation, the histograms represent the number of internodes in each category compared with the number of internodes of the plant under optimal environmental conditions, i.e. the percentage of optimum internodes).

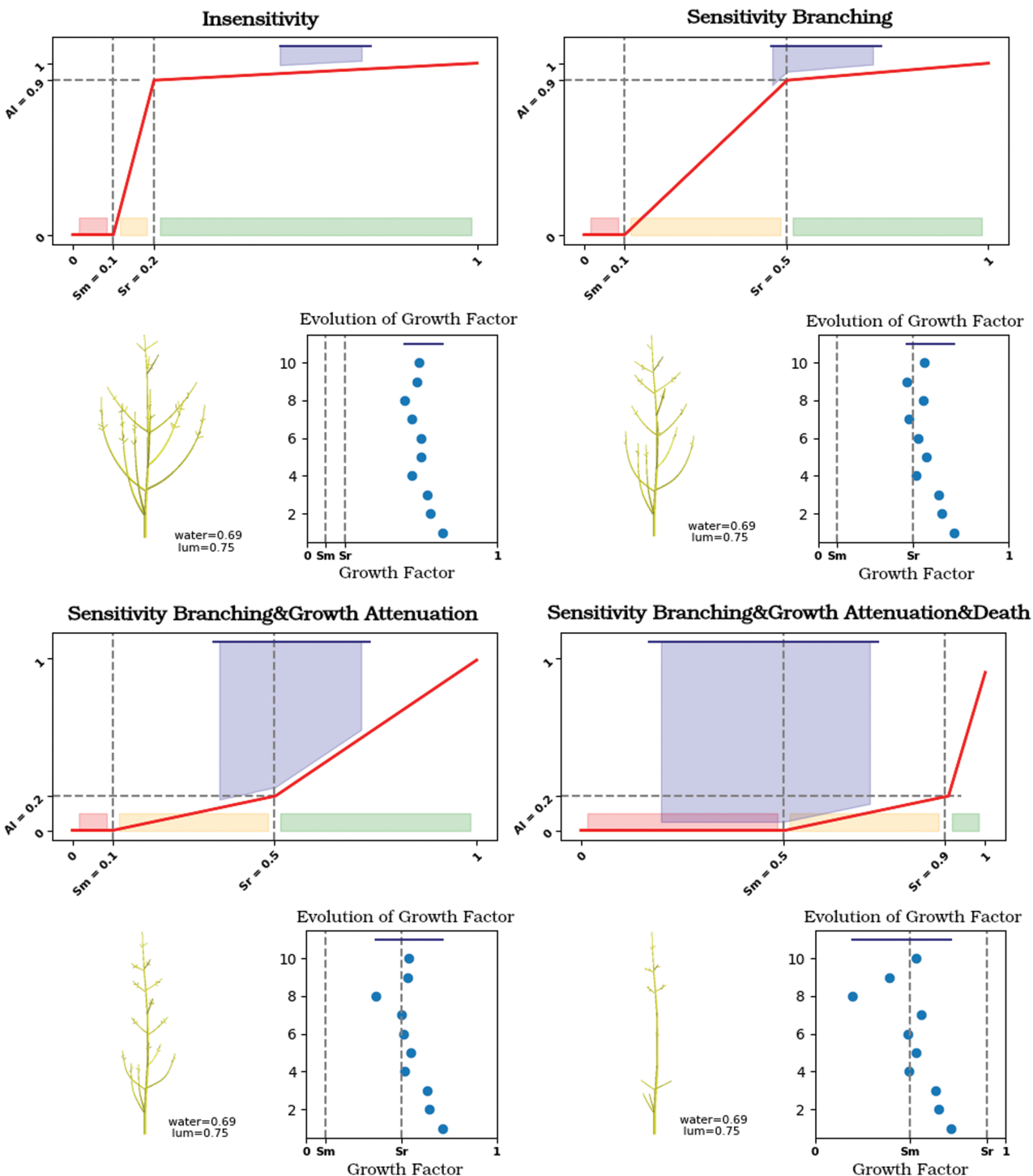


Figure 7. Four examples of possible threshold and attenuation functions (TAF) modelling the response of a functional axis category to variation of the growth factor. The grey zone in the attenuation function curves shows the range of growth factor values throughout the corresponding simulation.

attenuation between the branching and the non-branching zone of the growth factor. The higher the value of  $A_l$ , the less sensitive it is to values of the growth factor greater than  $S_r$  and the more sensitive it is

to values of the growth factor between  $S_m$  and  $S_r$  (Fig. 7, upper two cases). The lower the value of  $A_l$ , the more sensitive it is to values of the growth factor greater than  $S_r$  and the less sensitive it is to values of the

growth factor between  $S_m$  and  $S_r$  (Fig. 7, lower two cases). Parameter  $S_r$  controls branching. The lower the value of  $S_r$ , the larger the number of branches (Fig. 7, case in the upper left with many short axes). The higher the value of  $S_r$ , the fewer branches (other cases with a few short axes). Parameter  $S_m$  controls axis mortality. The higher the value of  $S_m$ , the fewer the living axes in this category (Fig. 7, lower right case). The lower the value of  $S_m$ , the larger the number of living axes (Fig. 7, other cases).

It is easy to grasp the huge number of possible combinations available to define different genotypes and plant sensitivity to environmental constraints by varying the  $6 \times 3$  parameter values. The modeller can define them manually based on his/her knowledge. Another possible way would be to use a calibration tool able to predict the correct values of the parameters of the model based on measurements.

### 3.2 Calibration results

In this section, we present the results of implementing the calibration method (see section 2.2). The calibration method relies on training the VoxNet neural network on simulated data. The results of calibrating the TOY model are thus to be understood as predictions made by the trained VoxNet neural networks. We also assessed the quality of VoxNet predictions using simulated data (see section 2.2.4).

**3.2.1 Calibration of the three hidden parameters of the TOY first functional shoot category** The aim of the calibration method was to

assess TOY hidden parameter values. The TOY hidden parameters are the parameters of endogenous growth processes, i.e. the death threshold  $S_m$ , the branching threshold  $S_r$  and the apical growth factor  $A_l$  for each functional axis category (see Table 1). Figure 8 shows the results of the training calibration of the three hidden parameters for the shoot first functional category on SubDBStress (A) (see section 2.2.3) and on the whole training data set (B). Similar results were obtained for the five other functional categories.

With a median RApE of 1.3 % for  $A_l$ , 0.8 % for  $S_r$  and 4.2 % for  $S_m$ , the predictions made by VoxNet trained on SubDBStress are fully accurate for the test examples under water and light stress. With a median RApE of 1.3 % for  $A_l$ , 0.7 % for  $S_r$  and 5.0 % for  $S_m$ , they are also highly accurate for the test examples under water stress alone. This result underlines the greater sensitivity of the TOY model to water availability than to light availability. Indeed, with a median RApE of 28.5 % (resp. 37.6 %) for  $A_l$ , 19.2 % (resp. 35.8 %) for  $S_r$  and 32.0 % (resp. 46.4 %) for  $S_m$ , the predictions given by VoxNet trained on SubDBStress showed very poor accuracy for the test examples under light stress alone, and were very close to random for the test examples under no stress. Altogether the quality of the predictions made by VoxNet trained on SubDBStress was poor, with a mean RApE on the whole test data set of 24 % for  $A_l$ , 19 % for  $S_r$  and 30 % for  $S_m$ .

(b) The quality of the predictions by VoxNet trained on the whole training data set fine-tuned with the weights of the training on SubDBStress was significantly better, with a mean RApE on the whole

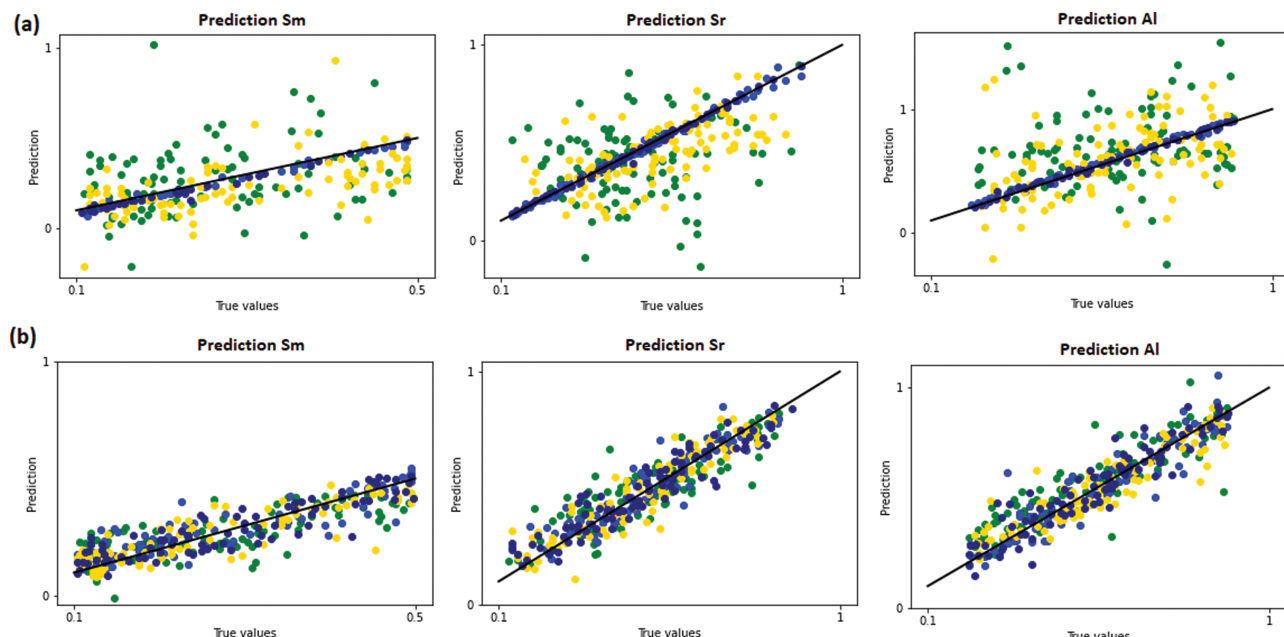


**Figure 8.** Predicted versus true values of the three hidden parameters modelling the death threshold, the branching threshold and the apical growth factor of the shoot in the first functional axis category. (A) VoxNet trained on the sub-data set of examples under water and light stress. (B) VoxNet trained on the whole training data set, fine-tuned using the weights of the training on SubDBStress. Each graph displays 400 examples of the test database. The colours stand for the environmental conditions of the examples: dark blue for water and light stress, blue for water stress alone, yellow for light stress alone and green for no environmental stress. The black solid line represents the 1:1 line.

test data set of 13 % for  $A_l$ , 14 % for  $S_r$  and 22 % for  $S_m$ . The predictions made by VoxNet trained on the whole data set for example, under water stress alone or under both water and light stress were still slightly more accurate than the predictions made for examples under light stress or no stress at all. However, they were significantly more accurate than the predictions made by the previous VoxNet trained on *SubDBStress*. The overall improvement in the quality of predictions given by the VoxNet trained on the whole data set was driven by the notable improvement in the quality of the predictions for the test examples under light stress alone and under no stress. Indeed, in comparison with the previous training, the median RApE for the test examples under light stress alone (resp. no stress) decreased significantly from 28.5 to 7.5 % (resp. from 37.6 to 10.0 %) for  $A_l$ , from 19.2 to 9.0 % (resp. from 35.8 to 13.5 %) for  $S_r$  and from 32.0 to 18.1 % (resp. from 46.4 to 17.5 %) for  $S_m$ . Since the values of environmental parameters are included in some voxels of the voxelized representation of plant architectural development, the only explanation for this reduction in accuracy is that the information contained in those voxels is partially lost through convolution.

The results of both trainings share one similarity: the predictions of the values of the branching threshold  $S_r$  and the apical growth factor  $A_l$  were significantly more accurate than the prediction of the value of the mortality threshold  $S_m$ . This may be due to the fact that the three parameters do not modulate plant responses to the same degree of severity of the stress;  $A_l$  and  $S_r$  modulate plant responses to mild environmental stresses, whereas  $S_m$  modulates plant responses to more severe stresses. Since severe stresses, modelled by low values of the growth factor, are less frequent during and among the simulations that comprise the training data set, it is probably more difficult for VoxNet to learn how to predict the value of the mortality threshold  $S_m$ .

A particularly interesting result is the prediction that VoxNet is able to provide on the examples under limited stress. Even though the prediction is of low quality, the ability of the network to predict plant responses to environmental stresses based on an example in which the plant architecture developed in the absence of stress is quite remarkable. This result requires more detailed investigation. In particular, the definition of stress used to classify the examples is rather vague (decrease of at least 25 % in water (resp. light) availability compared to the optimum). It would be interesting to refine this definition, to be able to quantify the extent of VoxNet's ability to predict plant responses to environmental constraints based on the simulation of a plant facing few or no environmental constraints.

### 3.2.2 Calibration of the two parameters for light and water availability

**3.2.2.1 Calibration method inversion.** Endogenous growth processes are assumed to be identical amongst all individuals of the same plant species. As such, the values of the 18 hidden parameters of the TOY model for endogenous growth are assumed to be associated with the plant species. For a given plant species, once these 18 values have been assessed, phenotypic plasticity between individuals is assumed to be modulated only by the values of the environmental parameters and exogenous growth processes.

Since the environment is measurable, the values of the environmental parameters can be assessed using standard calibration methods. However, since it is possible to construct a large data set containing

architectural development simulations of an individual of a given species growing in different environmental constraints, it is also possible to train the VoxNet neural network to predict the environmental conditions under which the individual has developed.

For the purpose of inverting the calibration method, further training of VoxNet was undertaken. Eighteen hidden TOY model parameter values were fixed, as well as the three values of the parameters for exogenous growth processes. The fixed values of these parameters were carefully chosen, such that the resulting simulated individual expresses phenotypic plasticity, which, in turn, modifies its architectural development under different environmental constraints. Since most of the parameter values were fixed and only two values needed to be predicted, it was possible to reduce the size of the training data set to 20 000 examples. All the examples were constructed with the RoCoCau+TOY simulations of individuals under varying environmental constraints (for each simulation, the water and light availability values were chosen randomly between 0.5 and 1). The simulations were represented as voxelized density maps but without the two voxels in each structure representing water and light availability and labelled with the true values of the two parameters for water and light availability (see section 3). Finally, VoxNet architecture was slightly modified by reducing the size of the fully connected layer to 2, thus making it possible to predict two instead of three parameter values.

**3.2.2.2 Results.** The predictions given by the trained VoxNet shown in Fig. 9 are fully accurate for every example of the test data set, with a mean RApE of 1.5 % for light availability, and of 2 % for water availability. The results of the inversion of the calibration method are therefore conclusive: they demonstrate VoxNet's ability to accurately predict the impact of water and light availability on the architectural development of a given individual of a given species.

## 4. DISCUSSION

In this section, we first discuss the main limitations and possible improvements of the TOY model. As the model is still in its early stages of development, the discussion is not intended to be exhaustive but rather to identify avenues for immediate improvement. We then discuss the method of calibration, mostly focusing on possible improvements to the calibration of current and future versions of the TOY model.

Throughout the conception of the calibration method for the TOY model, particular emphasis was placed on (i) minimizing the quantity of laborious tree architectural measurements to be performed for the calibration and (ii) separating the calibration of parameter values for the environment, and for exogenous and endogenous processes, so that RoCoCau+TOY FSPM can be calibrated to simulate phenotypic plasticity (Fig. 4). With respect to these two constraints, we propose a procedure for the calibration and use of RoCoCau+TOY FSPM based on measurements on a single *in vivo* tree.

### 4.1 Limitations and possible improvements of the TOY model

The main objective of this study was to build a modelling framework able to (i) accurately simulate whole tree growth, with particular attention paid to the interdependencies between the root and shoot

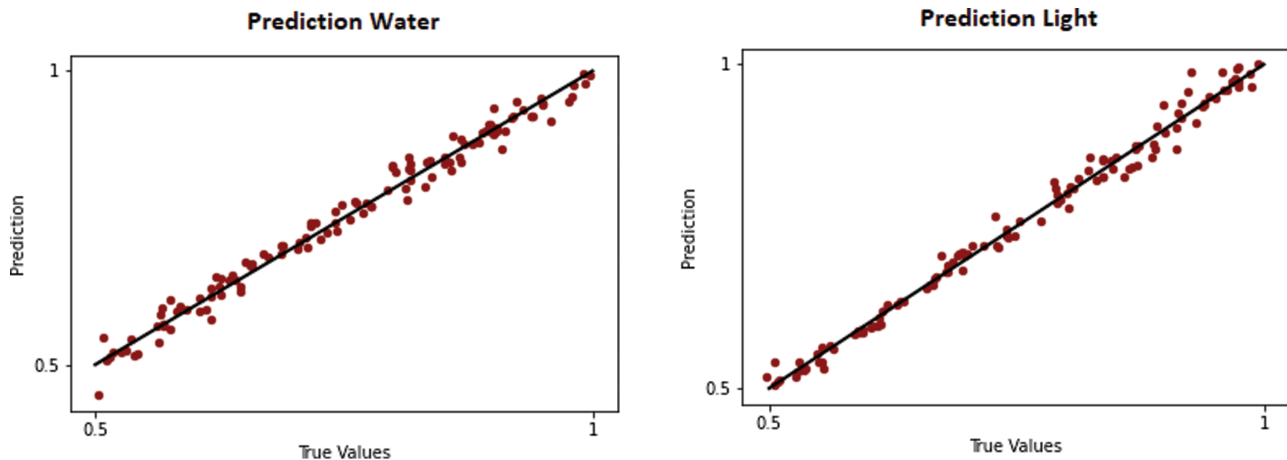


**Figure 9.** Predicted versus true values of the two parameters for light and water availability. Each graph displays 120 examples from the test database. The solid black line represents the 1:1 line.

compartments and (ii) to untangle genotype and environment effects on architectural development to predict phenotypic plasticity. Since such a modelling framework will be useful for a wide range of tree species when linked to RoCoCau, the TOY model can be applied to any type of tree and its set-up is therefore mainly focused on its genericity and precision rather than on its physiological realism. We also discuss the genericity of RoCoCau+TOY FSPM in this section.

The first limitation of RoCoCau+TOY FSPM is the independence of the six-axis functional categories. It will be recalled that we chose six functional categories to express the structuring, exploration and exploitation processes that occur during plant growth. However, more structural categories may be needed to describe the architectural unit of a species. For each of the six functional categories the RoCoCau simulator modulates axes development independently, giving RoCoCau+TOY FSPM high genericity. However, such independence is not realistic, since the growth of all the axes is subject to biomass conservation, i.e. the cumulated biomass of all the new axes and of all the new portions of axes at a particular time step is equal to the amount of biomass allocated to tree growth. For RoCoCau+TOY FSPM to account for biomass conservation, the TOY model thus needs to be refined. Biomass sharing between functional axis categories can be explicitly written to express the strategy used by the plant species to face stresses over time (for instance, pioneer trees that mainly invest in trunk growth, whereas shade tolerant trees prefer to invest in lateral branches; Cai *et al.* 2013; Coll *et al.* 2008; Delagrange *et al.* 2008; Henry *et al.* 2010). It could also be improved by adding equations to estimate the amounts of biomass allocated for other essential functions of the tree, i.e. reserve, maintenance, reproduction and defence.

The second limitation concerns the branching process, which is mainly managed by the RoCoCau software. Indeed, axes of the first and the second categories can branch into new axes at each time step, the probabilities being fixed by the RoCoCau software. Within RoCoCau+TOY FSPM, the TOY model gives a binary modulation to those branching probabilities. It sets them to zero when the value of the growth factor is below the branching threshold. A first refinement of TOY model could consist in implementing continuous modulation of the branching probabilities, e.g. a linear decrease in the branching probability following the decrease in the growth factor. A more important refinement however, concerns the

branching of the axes of the first functional category, e.g. the trunk and taproot. Indeed, axes of the first functional category can branch into axes of the second or the third category, e.g. branches or short shoots, lateral roots and fine roots, with different degrees of probability. It is likely that trees can modulate the branching process towards the second or the third category, towards exploration or exploitation, depending on the environment. Given that, the two probabilities are fixed by the RoCoCau software, and simultaneously set to zero when the growth factors value drops below the branching threshold, the RoCoCau+TOY FSPM is currently not able to account for new axis strategies, which reduces its genericity. The FSPM could be improved by adding new equations to the TOY model to allow it to modulate the two branching probabilities of the first category based on the environmental constraints.

The third limitation concerns modelling the environment, in particular the soil compartment, which is rudimentary in the current version of the FSPM. Indeed, the impact of the soil compartment on tree growth, and biomass partitioning is currently limited to water availability, which is itself considered homogeneous and is represented by the constant parameter  $Hv_{soil}$ . The first refinement to the TOY model therefore concerns spatialization of soil water availability, e.g. by representing the soil compartment as a set of layers or a 3D grid of cells containing different water availabilities, as frequently observed in the field (Manoli *et al.* 2014; Braghieri *et al.* 2020).

Finally, as shown in Reynolds and D'Antonio (1996) and Poorter *et al.* (2012), nutrient availability is a determining parameter of the optimal partitioning theory (Reich 2002). It has a significant impact on tree biomass partitioning between the root and shoot compartments and on growth processes. Another refinement of the TOY model should therefore be including nutrient availability, as in McMurtie and Landsberg (1992), Reynolds and D'Antonio (1996), and Lacander *et al.* (2021).

## 4.2 Limitations and possible improvements of the calibration method

**4.2.1 Analysis** We chose a neural network suited to our specific task and improved it. Each plant growth simulation produces a 3D voxel image that contains 10 growth time steps split between the woody and

absorbing parts. It is currently possible to predict  $6 \times 3$  hidden TOY parameter values with acceptable accuracy after training on a simulated data set, which is a very promising result. As the input of the network consists in a voxelized representation of the plant, it is independent of the model to be inverted. It is thus possible to keep the same neural network to calibrate future improved versions of TOY.

VoxNet was chosen for calibration because of its 3D input and because it is simple to adapt for generative purposes. It is clear that including time series in a single 3D image may not be the most accurate way to calibrate a dynamic model, not to mention including light and water availability in some voxels. It would thus be interesting to test recurrent networks whose structure natively includes this time feature. Another possible improvement would be to compute the loss according to the distance between the 3D images obtained from the target parameter values and from the predicted value rather than on the distance between the original and predicted parameter values. This will require calibrating all parameters in the same model, which was not possible for us due to hardware restrictions. Calibration will also be improved and tested further by our team, especially on yearly variations in the environment and using multiresolution 3D inputs rather than a single 3D input.

**4.2.2 Future outlook** Although time series of environmental conditions can be used as inputs for the TOY model, thus accounting for inter-annual variability, the current architecture of the VoxNet neural network only allows the prediction of a single value for the parameters that influence light and water availability. As VoxNet is already able to predict the impact of a permanent stress on individual plant architectural development very accurately (see section 4.2), it would be interesting to introduce recurrence into its architecture (Medsker and Jain 2000; Liang and Hu 2015; Zuo *et al.* 2015), to enable it to predict time series of changing environmental parameter values, and also to test if it is able to predict the impact of episodic stresses. For instance, what would the difference in the final plant architecture be if it were affected by a single year of drought at the beginning or at the end of plant life (Backhaus *et al.* 2014).

Another improvement would be increasing the size of the input layer of the network to be able to process bigger or more complex trees. In this study, only the output of the network was adapted to make it generative. Also, the accuracy of the prediction was checked using the values of the predicted parameters. It would be interesting to compare the simulation run with the predicted values with the original tree. A more complex way would be to replace a single VoxNet with a single input 3D voxel image containing 10 growth time steps with a set of 10 VoxNets, each of which has an input of the corresponding shape at this time step, and each of the 10 VoxNets would be fully connected at the last layer. A big improvement in this strategy would be to adapt the resolution of each of the 10 3D images according to the current size of the growing plant, thus providing a more accurate input at each time step.

The next important step will be to test the method on real plants. This can be achieved through simulations of RoCoCau after calibration based on architectural measurements made in particular species. Predictions could then be made according to the reconstructed target. Yet another way would be to use LiDAR images converted into

voxel 3D images as inputs. The second solution would avoid mock-up simulations and probably match reality better. This solution would only apply to the shoot system because no device is currently available to capture the root system without uprooting it. Some technologies including mini-rhizotrons, micro-x-ray chromatography CT, nuclear magnetic resonance (NMR imaging) and positron emission tomography (PET) are already capable of that (Huck and Taylor 1982; Cassidy Steven *et al.* 2020; Peruzzo *et al.* 2020) but are mainly used for small plants. Non-destructive observation of root growth of large plants at field scale still remains challenging despite recent attempts using radar (Hruska *et al.* 1999; Barton and Montagu 2004; Alani and Lantini 2020).

Another interesting use of RoCoCau+TOY with its calibration neural network could be to guess the characteristics of the root system with a known shoot system and known environmental conditions. Knowledge of the extension and depth of a root system is indispensable, especially for tree management in urban environments (Randrup *et al.* 2001; Bartens *et al.* 2008; Bartens *et al.* 2009). Calibration and use of RoCoCau+TOY FSPM based on measurements of a single phenotype.

The purpose of RoCoCau+TOY FSPM is to predict the architectural development of an individual of a given tree species under varying environmental conditions, in other words to predict phenotypic plasticity. To check the quality of RoCoCau+TOY FSPM predictions, measurements of several tree phenotypes are required, meaning measurements have to be taken on several tree stands growing in significantly different environments, as is the case in studies of shoot organogenesis and axis organization (Stecconi *et al.* 2010; Taugourdeau and Sabatier 2010; Sabatier *et al.* 2011; Taugourdeau *et al.* 2011, 2012; Buissart *et al.* 2018). However, since the TOY model is based on the disentanglement of genome and environment ( $G \times E$ ) interactions, the calibration and use of the RoCoCau+TOY FSPM only require measurements on a single phenotype, hence on a single tree stand.

**4.2.3 Calibrating the RoCoCau simulator** Calibrating the RoCoCau simulator for a given tree phenotype requires extensive measurements of architectural traits throughout the architectural development of the tree. As measuring root architectural traits is destructive, measurements have to be made on several trees belonging to the same species and sharing the same environment (at least one tree per architectural development stage). These measurements are then used to calibrate the RoCoCau simulator, allowing it to accurately simulate a botanical representation of the architectural development of a given tree phenotype. Measurement of whole-plant architecture is rare, some approaches with automatic devices are available but only for use on very simple herbaceous plants (Nagel *et al.* 2012).

**4.2.4 Calibrating TOY parameters for exogenous growth on a single phenotype** TOY parameters for exogenous growth are (i) two parameters of the light absorption equation: the light extinction coefficient  $k$ , and the maximum useable light energy  $Light_{max}$  ( $\text{w} \cdot \text{m}^{-2}$ ), and (ii) the parameter of the water uptake equation: root absorbing length ( $RAL$ ) and radius of absorbing soil  $R_{||}$  (see Table 1). Light extinction coefficient  $k$  and  $Light_{max}$  parameters can be obtained by fitting the

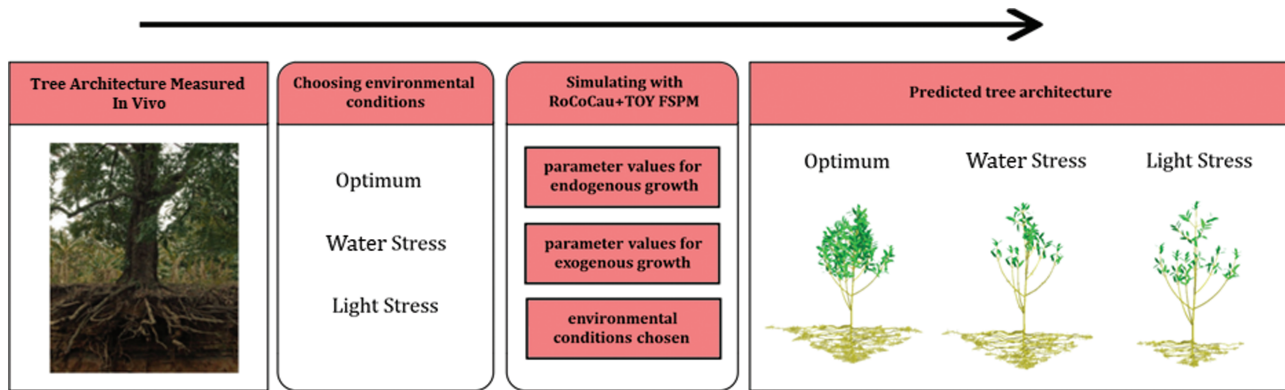


**Figure 10.** Predicting *in vivo* tree architecture under varying environmental conditions using RoCoCau+TOY FSPM, based on measurements made on a single *in vivo* tree stand for the calibration of RoCoCau simulator and TOY model.

Beer–Lambert equation with measurements of photosynthetic active radiation (PAR) above, within and under the canopy, completed with the leaf area index (LAI). The root absorbing length (RAL) can be measured directly on the roots of uprooted trees during calibration of RoCoCau. The radius of absorbing soil  $R_{\parallel}$  can be obtained from the literature or from measurements (Nadezhina and Cermak 2003; Corners and Leuschner 2005).

More detailed equations for water uptake and light absorption are available in the literature (Reynolds and Thorne 1982; McMurtrie and Landsberg 1992) and could be used to improve the TOY model. However, it is important to point out that the TOY model relies on the disentanglement of genotype and environmental effects. The unambiguity of the TOY model is a precondition of its ability to predict phenotypic plasticity. When improving or replacing TOY equations for exogenous growth, it is therefore preferable to use only parameters whose calibration is not specific to the observed phenotype, parameters depicting either tree genotype or the environment.

**4.2.5 Calibrating TOY parameters for endogenous growth of the tree species on a single phenotype** The 18 TOY hidden parameters for endogenous growth are the focus of the calibration method developed in this study (see section 3). Once the RoCoCau simulators and the exogenous growth parameters are calibrated, it is possible to implement RoCoCau+TOY FSPM with random endogenous growth parameters to build a simulated training data set and to train VoxNet neural networks to predict the values of the endogenous growth parameters.

Since the output formats of RoCoCau and RoCoCau+TOY FSPM are the same, it is possible to provide the trained VoxNet neural networks with a voxelized density map of the RoCoCau simulation of the tree phenotype measured *in vivo* (see section 5.1.1). The prediction given by the trained VoxNet neural networks for this input are the values of the endogenous growth parameters for the tree species measured *in vivo*.

**4.2.6 Predicting *in vivo* tree architectural development under varying environmental conditions using RoCoCau+TOY FSPM** Once the RoCoCau simulator and the TOY model have been calibrated, the use of RoCoCau+TOY FSPM relies on the modeller's choice of

environmental conditions. Provided with the calibrated values of exogenous growth parameters, the calibrated values of endogenous growth parameters and the chosen values for environment parameters, the RoCoCau+TOY FSPM can predict the architecture of tree measured *in vivo* if it had grown in the chosen conditions instead of in the actual environmental conditions. The RoCoCau+TOY FSPM can predict the phenotypic plasticity of the tree measured *in vivo* (Fig. 10).

## 5. CONCLUSION

RoCoCau is a new structural whole-plant growth model (describing shoot and root growth and their interactions at the same time). It includes an approach using the architectural unit concept and relies on structural axis categories. Basic functions that explain growth (apical growth, branching, death and self-pruning) are adapted to our specific field of knowledge and experimental measurements made in the shoot and root compartments (Taugourdeau *et al.* 2012). The RoCoCau simulator can produce 3D mock-ups that are botanically accurate. The functional TOY module is dynamically linked to RoCoCau to express shoot-root compartment dependencies for:

- biomass production that requires carbon, water and light;
- partitioning to balance shoot and root compartments absorbing contributions and modulating further growth.

The combination RoCoCau+TOY produces an FSPM that can express a variety of growth strategies and reveal plant plasticity under varying environmental conditions.

It is possible to fit RoCoCau to a particular species thanks to measurements on both compartments but most of the 25 parameters of TOY are hidden parameters with values that can only be calibrated using numerical tools. It is possible but unlikely that such a large number of values can be discovered using standard methods, which is why we tested the capability of neural networks to accomplish this task. To this end, we adapted the well-known VoxNet convolutional neural network and tested the quality of its predictions using simulated plant data sets for training and validation. The input of the network consists in a 3D voxel representation of split woody and absorbing parts of the

plant and the output consists in sets of three values of TOY hidden parameters. The method predicted  $6 \times 3$  TOY hidden parameter values with a very good accuracy after training on a simulated data set and fine-tuning.

The next steps in this project will consist in improvements in two complementary directions. In the biological field, the TOY model will be improved to better match plant knowledge, which needs to be achieved while keeping TOY as simple and compact as possible. The TOY model should include new important features such as nitrogen contribution (Kobe *et al.* 2010; Liu *et al.* 2012); better management of the soil or biomass reserves. On the other hand, many actions need to be performed in the numerical and computer science field to improve calibration. The use of convolutional neural networks is promising, but the VoxNet was adapted for TOY calibration in a simple way while changing the last fully connected layer and using a single 3D image containing both a plant growth time sequence and climate values. We are aware that recurrent networks are considered to be more accurate for processing time series. The input content and the loss computing can also be improved. The last step will consist in using real species. The main idea is that, thanks to the botanical accuracy of RoCoCau, it will be possible to replicate plant architecture based on simplified measurements and to train the network on simulated data sets with random values of TOY and then to predict TOY model parameter values that match measured values.

## CONTRIBUTIONS BY THE AUTHORS

A.L.M. mainly cared about the calibration part and VoxNet input/output data content. He also helped about RoCoCau+TOY check and improvement. E.N. and Y.C. brought their knowledge about plants. P.B. brought his knowledge about neural network theory and technical management. J.-F.B. built RoCoCau+TOY model and simulator according to E.N. and Y.C. knowledge, provided the training/validation databases and coordinated the study.

## DATA AVAILABILITY

The source code of the RoCoCau simulator with the plant parameter files used for this study is available on <http://amapstudio.cirad.fr/>. The source code of the neural network calibration tool can be downloaded from [https://github.com/AbelMasson/VoxNet\\_Strat](https://github.com/AbelMasson/VoxNet_Strat).

## LITERATURE CITED

- Alani AM, Lantini L. 2020. Recent advances in tree root mapping and assessment using non-destructive testing methods: a focus on ground penetrating radar. *Surveys in Geophysics* **41**:605–646.
- Backhaus S, Kreyling J, Grant K, Beierkuhnlein C, Walter J, Jentsch A. 2014. Recurrent mild drought events increase resistance toward extreme drought stress. *Ecosystems* **17**:1068–1081.
- Bacour C, Baret F, Béal D, Weiss M, Pavageau K. 2006. Neural network estimation of LAI, FAPAR, fCover and LAI×Cab, from top of canopy MERIS reflectance data: principles and validation. *Remote Sensing of Environment* **105**:313–325.
- Ballaré CL, Pierik R. 2017. The shade-avoidance syndrome: multiple signals and ecological consequences. *Plant, Cell & Environment* **40**:2530–2543.
- Barczi JF, Rey H, Caraglio Y, de Reffye P, Barthélémy D, Dong QX, Fourcaud T. 2008. AmapSim: a structural whole-plant simulator based on botanical knowledge and designed to host external functional models. *Annals of Botany* **101**:1125–1138.
- Barczi JF, Rey H, Griffon S, Jourdan C. 2018. DigR: a generic model and its open source simulation software to mimic three-dimensional root-system architecture diversity. *Annals of Botany* **121**:1089–1104.
- Bartens J, Day SD, Harris JR, Dove JE, Wynn TM. 2008. Can urban tree roots improve infiltration through compacted subsoils for stormwater management?. *Journal of Environmental Quality* **37**:2048–2057.
- Bartens J, Day SD, Harris JR, Wynn TM, Dove JE. 2009. Transpiration and root development of urban trees in structural soil stormwater reservoirs. *Environmental Management* **44**:646–657.
- Barthélémy D, Caraglio Y. 2007. Plant architecture: a dynamic, multilevel and comprehensive approach to plant form, structure and ontogeny. *Annals of Botany* **99**:375–407.
- Barton CVM, Montagu KD. 2004. Detection of tree roots and determination of root diameters by ground penetrating radar under optimal conditions. *Tree Physiology* **24**:1323–1331.
- Bornhofen S, Lataud C. 2007. Evolution of virtual plants interacting with their environment. In: Proceedings of VRIC. Laval, France, 172–176.
- Braghiere RK, Gérard F, Evers JB, Pradal C, Pages L. 2020. Simulating the effects of water limitation on plant biomass using a 3D functional-structural plant model of shoot and root driven by soil hydraulics. *Annals of Botany* **126**:713–728.
- Buck-Sorlin G. 2013. Process-based model. In: Dubitzky W, Wolkenhauer O, Cho K-H, Yokota H, eds. *Encyclopedia of systems biology*. New York, NY: Springer, 1755–1755.
- Buck-Sorlin G, de Visser PH, Henke M, Sarlikioti V, van der Heijden GW, Marcelis LF, Vos J. 2011. Towards a functional-structural plant model of cut-rose: simulation of light environment, light absorption, photosynthesis and interference with the plant structure. *Annals of Botany* **108**:1121–1134.
- Buissart F, Vennetier M, Delagrange S, Girard F, Caraglio Y, Sabatier SA, Munson AD, Nicolini EA. 2018. The relative weight of ontogeny, topology and climate in the architectural development of three North American conifers. *AoB Plants* **10**:ply045; doi:[10.1093/aobpla/ply045](https://doi.org/10.1093/aobpla/ply045).
- Cai S, Kang X, Zhang L. 2013. Allometric models for aboveground biomass of ten tree species in northeast China. *Annals of Forest Research* **56**:105–122.
- Cassidy Steven T, Burr AA, Reeb RA, Melero Pardo AL, Woods KD, Wood CW. 2020. Using clear plastic CD cases as low-cost mini-rhizotrons to phenotype root traits. *Applications in Plant Sciences* **8**:e11340.
- Coll L, Potvin C, Messier C, Delagrange S. 2008. Root architecture and allocation patterns of eight native tropical species with different successional status used in open-grown mixed plantations in Panama. *Trees* **22**:585–596.
- Colter Burkes E, Will RE, Barron-Gafford GA, Teskey RO, Shiver B. 2003. Biomass partitioning and growth efficiency of intensively managed *Pinus taeda* and *Pinus elliottii* stands of different planting densities. *Forest Science* **49**:224–234.

- Corners H, Leuschner C. 2005. In situ measurement of fine root water absorption in three temperate tree species—temporal variability and control by soil and atmospheric factors. *Basic and Applied Ecology* **6**:395–405.
- Côté J-F, Widlowski J-L, Fournier RA, Verstraete MM. 2009. The structural and radiative consistency of three-dimensional tree reconstructions from terrestrial lidar. *Remote Sensing of Environment* **113**:1067–1081.
- Cournède P-H, Letort V, Mathieu A, Kang MZ, Lemaire S, Trevezas S, Houllier F, de Reffye P. 2011. Some parameter estimation issues in functional-structural plant modelling. *Mathematical Modelling of Natural Phenomena* **6**:133–159.
- Danson FM, Rowland CS, Baret F. 2003. Training a neural network with a canopy reflectance model to estimate crop leaf area index. *International Journal of Remote Sensing* **24**:4891–4905.
- de Reffye P, Edelin C, Françon J, Jaeger M, Puech C. 1988. Plant models faithful to botanical structure and development. *ACM SIGGRAPH Computer Graphics* **22**:151–158.
- de Reffye P, Houllier F, Cournède P-H. 2016. Méthodes inverses et identification paramétrique de modèles d'architecture végétale. In: *Architecture et croissance des plantes. Modélisation et applications, synthèses*, 978-27592-2622-1. hal-02539715.
- de Reffye P, Hu B, Kang M, Letort V, Jaeger M. 2021. Two decades of research with the GreenLab model in agronomy. *Annals of Botany* **127**:281–295.
- de Reffye P, Jaeger M, Sabatier S, Letort V. 2018. Modelling the interaction between functioning and organogenesis in a stochastic plant growth model: methodology for parameter estimation and illustration. In: 2018 6th International Symposium on Plant Growth Modeling, Simulation, Visualization and Applications (PMA), Hefei, China. 102–110.
- Delagrange S, Potvin C, Messier C, Coll L. 2008. Linking multiple-level tree traits with biomass accumulation in native tree species used for reforestation in Panama. *Trees* **22**:337–349.
- Doussan C, Pierret A, Garrigues E, Pagès L. 2006. Water uptake by plant roots: II—modelling of water transfer in the soil root-system with explicit account of flow within the root system—comparison with experiments. *Plant and Soil* **283**:99–117.
- Estornell J, Hadas E, Martí J, López-Cortés I. 2021. Tree extraction and estimation of walnut structure parameters using airborne LiDAR data. *International Journal of Applied Earth Observation and Geoinformation* **96**:102273.
- Fan G, Nan L, Chen F, Dong Y, Wang Z, Li H, Chen D. 2020. A new quantitative approach to tree attributes estimation based on LiDAR point clouds. *Remote Sensing* **12**:1779.
- Ferrara R, Virdis SGP, Ventura A, Ghisu T, Duce P, Pellizzaro G. 2018. An automated approach for wood-leaf separation from terrestrial LiDAR point clouds using the density based clustering algorithm DBSCAN. *Agricultural and Forest Meteorology* **262**:434–444.
- Friend A. 2001. Modelling canopy CO<sub>2</sub> fluxes: are ‘big-leaf’ simplifications justified? *Global Ecology and Biogeography* **10**:603–619.
- Garrigues E, Doussan C, Pierret A. 2006. Water uptake by plant roots: I—formation and propagation of a water extraction front in mature root systems as evidenced by 2D light transmission imaging. *Plant and Soil* **283**:83–98.
- Henry M, Besnard A, Asante WA, Eshun J, Adu-Bredu S, Valentini R, Bernoux M, Saint-André L. 2010. Wood density, phytomass variations within and among trees, and allometric equations in a tropical rainforest of Africa. *Forest Ecology and Management* **260**:1375–1388.
- Hertel D, Strecker T, Müller-Haubold H, Leuschner C. 2013. Fine root biomass and dynamics in beech forests across a precipitation gradient—is optimal resource partitioning theory applicable to water-limited mature trees? *Journal of Ecology* **101**:1183–1200.
- Higgins SI, Scheiter S, Sankaran M. 2010. The stability of African savannas: insights from the indirect estimation of the parameters of a dynamic model. *Ecology* **91**:1682–1692.
- Hommel R, Siegwolf R, Zavadlav S, Arend M, Schaub M, Galiano L, Haeni M, Kayler ZE, Gessler A. 2016. Impact of interspecific competition and drought on the allocation of new assimilates in trees. *Plant Biology* **18**:785–796.
- Huck MG, Taylor HM. 1982. The rhizotron as a tool for root research. *Advances in Agronomy* **35**:1–35.
- Hruska J, Čermák J, Šustek S. 1999. Mapping tree root systems with ground-penetrating radar. *Tree Physiology* **19**:125–130.
- Jungk A. 2001. Root hairs and the acquisition of plant nutrients from soil. *Journal of Plant Nutrition and Soil Science* **164**:121–129.
- King DA. 1991. The allometry of trees in temperate and tropical forests. *National Geographic Research and Exploration* **7**:342–351.
- Kobe RK, Iyer M, Walters MB. 2010. Optimal partitioning theory revisited: nonstructural carbohydrates dominate root mass responses to nitrogen. *Ecology* **91**:166–179.
- Kurth W. 1994. Morphological models of plant growth: possibilities and ecological relevance. *Ecological Modelling, State-of-the-Art in Ecological Modelling Proceedings of ISEM's 8th International Conference* **75–76**:299–308.
- Lacander K, Zanchi G, Akselsson C, Belyazid S. 2021. The effect of nitrogen fertilization on tree growth, soil organic carbon and nitrogen leaching—a modeling study in a steep nitrogen deposition gradient in Sweden. *Forests* **12**:298.
- Lachenbruch B, McCulloh KA. 2014. Traits, properties, and performance: how woody plants combine hydraulic and mechanical functions in a cell, tissue, or whole plant. *The New Phytologist* **204**:747–764.
- ledo A, Paul KI, Burslem DFRP, Ewel JJ, Barton C, Battaglia M, Brooksbank K, Carter J, Eid TH, England JR, Fitzgerald A, Jonson J, Mencuccini M, Montagu KD, Montero G, Mugasha WA, Pinkard E, Roxburgh S, Ryan CM, Ruiz-Peinado R, Sochacki S, Specht A, Wildy D, Wirth C, Zerihun A, Chave J. 2018. Tree size and climatic water deficit control root to shoot ratio in individual trees globally. *The New Phytologist* **217**:8–11.
- Leitner D, Klepsch S, Bodner G, Schnepf A. 2010. A dynamic root system growth model based on L-systems. *Plant and Soil* **332**:177–192.
- Liang M, Hu X. 2015. Recurrent convolutional neural network for object recognition. In: Proceedings of the IEEE conference on computer vision and pattern recognition 3367–3375.
- Liu B, Cheng L, Li M, Liang D, Zou Y, Ma F. 2012. Interactive effects of water and nitrogen supply on growth, biomass partitioning, and water-use efficiency of young apple trees. *African Journal of Agricultural Research* **7**:978–985.
- Liu M, Han Z, Chen Y, Liu Z, Han Y. 2021. Tree species classification of LiDAR data based on 3D deep learning. *Measurement* **177**:109301.

- Mak H, Hu B. 2015. Characterization of tree structures from mobile LiDAR data for the identification of ASH trees. In: 2015 IEEE International Geoscience and Remote Sensing Symposium (IGARSS) (pp. 5371–5374). IEEE.
- Manoli G, Bonetti S, Domec JC, Putti M, Katul G, Marani M. 2014. Tree root systems competing for soil moisture in a 3D soil–plant model. *Advances in Water Resources* **66**:32–42.
- Matsunaga T, Hoyano A, Kobayashi H. 2001. Toward the inversion of vegetation parameters using canopy reflectance models. In: Smith WL, Yasuoka Y, eds. *Hyperspectral remote sensing of the land and atmosphere*. Bellingham, Washington: International Society for Optics and Photonics, 265–276.
- Maturana D, Scherer S. 2015. VoxNet: a 3D convolutional neural network for real-time object recognition. In: 2015 2015 IEEE/RSJ International Conference on Intelligent Robots and Systems (IROS) 922–928. IEEE.
- Mäyrä J, Keski-Saari S, Kivinen S, Tanhuanpää T, Hurskainen P, Kullberg P, Poikolainen L, Viinikka A, Tuominen S, Kumpula T, Vihervaara P. 2021. Tree species classification from airborne hyperspectral and LiDAR data using 3D convolutional neural networks. *Remote Sensing of Environment* **256**:112322.
- McMurtrie RE, Landsberg JJ. 1992. Using a simulation model to evaluate the effects of water and nutrients on the growth and carbon partitioning of *Pinus radiata*. *Forest Ecology and Management, The Biology of Forest Growth Experiment* **52**:243–260.
- Medsker LR, Jain LC. 2000. *Recurrent neural networks: design and applications, the CRC Press international series on computational intelligence*. Boca Raton, FL: CRC Press.
- Nadezhina N, Cermak J. 2003. Instrumental methods for studies of structure and function of root systems of large trees. *Journal of Experimental Botany* **54**:1511–1521.
- Nagel KA, Nagel KA, Putz A, Gilmer F, Heinz K, Fischbach A, Pfeifer J, Faget M, Blossfeld S, Ernst M, Dimaki C, Kastenholz B. 2012. GROWSCREEN-Rhizo is a novel phenotyping robot enabling simultaneous measurements of root and shoot growth for plants grown in soil-filled rhizotrons. *Functional Plant Biology* **39**:891–904.
- Niklas KJ, Enquist BJ. 2002. Canonical rules for plant organ biomass partitioning and annual allocation. *American Journal of Botany*, **89**:812–819.
- Nye PH. 1973. The relation between the radius of a root and its nutrient-absorbing power [ $\alpha$ ]: some theoretical considerations. *Journal of Experimental Botany* **24**:783–786.
- Pages L. 1999. Root system architecture: from its representation to the study of its elaboration. *Agronomie* **19**:295–304.
- Peruzzo L, Chou C, Wu Y, Schmutz M, Mary B, Wagner FM, Petrov P, Newman G, Blancaflor EB, Liu X, Ma X, Hubbard S. 2020. Imaging of plant current pathways for non-invasive root phenotyping using a newly developed electrical current source density approach. *Plant and Soil* **450**:567–584.
- Poorter H, Niklas KJ, Reich PB, Oleksyn J, Poot P, Mommer L. 2012. Biomass allocation to leaves, stems and roots: meta-analyses of interspecific variation and environmental control. *The New Phytologist* **193**:30–50.
- Postma JA, Kuppe C, Owen MR, Mellor N, Griffiths M, Bennett MJ, Lynch JP, Watt M. 2017. OpenSimRoot: widening the scope and application of root architectural models. *The New Phytologist* **215**:1274–1286.
- Qi CR, Su H, Nießner M, Dai A, Yan M, Guibas LJ. 2016. Volumetric and multi-view CNNs for object classification on 3D data. In: 2016 IEEE Conference on Computer Vision and Pattern Recognition (CVPR). 5648–5656.
- Randrup TB, McPherson EG, Costello LR. 2001. A review of tree root conflicts with sidewalks, curbs, and roads. *Urban Ecosystems* **5**:209–225.
- Reich PB. 2002. Root-shoot relations: optimality in acclimation and adaptation or the ‘Emperor’s new clothes’. In: Waisel Y, Eshel A, Kafkafi U, eds. *Plant roots: the hidden half*. New York: M. Decker, 314–338.
- Reyes F, Pallas B, Pradal C, Vaggi F, Zanotelli D, Tagliavini M, Gianelle D, Costes E. 2020. MuSCA: a multi-scale source–sink carbon allocation model to explore carbon allocation in plants. An application to static apple tree structures. *Annals of Botany* **126**:571–585.
- Reynolds HL, D’Antonio C. 1996. The ecological significance of plasticity in root weight ratio in response to nitrogen: opinion. *Plant and Soil* **185**:75–97.
- Reynolds JE, Thorne JHM. 1982. A shoot:root partitioning model. *Annals of Botany* **49**:585–597.
- Sabatier S, Andrianasolo DN, Rakotomalala JJ, Hamon P, De Reffye P, Letort V. 2011. *Plant architectural and genetic diversities in Coffea native from Madagascar: towards an architectural-functional plant growth model applied to Coffea biodiversity preservation*. BC2011. XVIII International Botanical Congress, 23–30 July 2011, Melbourne, Australia. [http://www.ibc2011.com/downloads/IBC2011\\_Abstract\\_Book.pdf](http://www.ibc2011.com/downloads/IBC2011_Abstract_Book.pdf).
- Sievänen R, Perttunen J, Nikinmaa E, Posada JM. 2009. Invited talk: functional structural plant models—case LIGNUM. In: 2009 Third International Symposium on Plant Growth Modeling, Simulation, Visualization and Applications 3–9. IEEE.
- Smith DD, Sperry JS, Enquist BJ, Savage VM, McCulloh KA, Bentley LP. 2014. Deviation from symmetrically self-similar branching in trees predicts altered hydraulics, mechanics, light interception and metabolic scaling. *The New Phytologist* **201**:217–229.
- Song S, Xiao J. 2016. Deep sliding shapes for Amodal 3D object detection in RGB-D images. In: Proceedings of the IEEE conference on computer vision and pattern recognition (CVPR). 808–816.
- Stecconi M, Puntieri J, Barthelemy D. 2010. An architectural approach to the growth forms of *Nothofagus pumilio* (Nothofagaceae) along an altitudinal gradient. *Botany* **88**:699–709.
- Su H, Maji S, Kalogerakis E, Learned-Miller E. 2015. Multi-view convolutional neural networks for 3D shape recognition. In: Proceedings of the IEEE international conference on computer vision (ICCV). 945–953.
- Taugourdeau O, Sabatier SA, Caraglio Y, Barthélémy D. 2011. *Morphogenetic gradients in silver firs (Abies alba Mill.) and their plasticity*. BC2011. XVIII International Botanical Congress, 23–30 July 2011, Melbourne, Australia. [http://www.ibc2011.com/downloads/IBC2011\\_Abstract\\_Book.pdf](http://www.ibc2011.com/downloads/IBC2011_Abstract_Book.pdf).
- Taugourdeau O, Dauzat J, Griffon S, Sabatier SA, Caraglio Y, Barthélémy D. 2012. Retrospective analysis of tree architecture in silver fir (*Abies alba* Mill.): ontogenetic trends and responses to environmental variability. *Annals of Forest Science* **69**:713–721.

- Taugourdeau O, Sabatier SA. 2010. Limited plasticity of shoot performance in response to light by understorey saplings of common walnut (*Juglans regia*). *AoB Plants*. **2010**:22.
- Vos J, Evers JB, Buck-Sorlin GH, Andrieu B, Chelle M, de Visser PH. 2010. Functional-structural plant modelling: a new versatile tool in crop science. *Journal of Experimental Botany* **61**:2101–2115.
- Vos J, Marcelis LFM, Evers JB. 2007. Functional-structural plant modelling in crop production: adding a dimension. *Frontis* **22**:1–12.
- Wandinger U. 2005. Introduction to lidar. In: Weitkamp C, eds. *Lidar: range-resolved optical remote sensing of the atmosphere*. New York, NY: Springer. 1–18.
- Zuo Z, Shuai B, Wang G, Liu X, Wang X, Wang B, Chen Y. 2015. Convolutional recurrent neural networks: learning spatial dependencies for image representation. In: Proceedings of the IEEE conference on computer vision and pattern recognition workshops 18–26.